Supporting Information for:

Understanding the Origin of Phosphorescence in Bismoles: A Synthetic and Computational Study

Sarah M. Parke,[†] Mary A. B. Narreto,[‡] Emanuel Hupf,[†] Robert McDonald,[†] Michael J. Ferguson,[†] Frank A. Hegmann,*[,‡] Eric Rivard*[,†]

[†]Department of Chemistry, University of Alberta, 11227 Saskatchewan Drive, Edmonton, Alberta, Canada T6G 2G2

[‡]Department of Physics, University of Alberta, Edmonton, Alberta, Canada T6G 2E1

Contents:

S4 **NMR Spectra**

S15 **X-ray Crystallographic Data**

S25 **Photoluminescence Data**

S30 **Computational Details**

Figures and Tables:

Figure S1: ^{1}H NMR spectrum of 1-phenyl-2,3,4,5-tetraethylbismole **1.**

Figure S2: ^{13}C{^{1}H} NMR spectrum of 1-phenyl-2,3,4,5-tetraethylbismole **1.**

Figure S3: ^{1}H NMR spectrum of 1-mesityl-2,3,4,5-tetraethylbismole **2**.

Figure S4: ^{13}C{^{1}H} NMR spectrum of 1-mesityl-2,3,4,5-tetraethylbismole **2**.

Figure S5: ^{1}H NMR spectrum of compound **3**.

Figure S6: ^{13}C{^{1}H} NMR spectrum of compound **3**.

Figure S7: ^{11}B{^{1}H} NMR spectrum of compound **3**.

Figure S8: ^{1}H NMR spectrum of dithienyl bismole **4**.

Figure S9: ^{13}C{^{1}H} NMR spectrum of dithienyl bismole **4**.

Figure S10: ^{1}H NMR spectrum of 1,2,3,4,5-pentaphenylbismole **5**.

Figure S11: ^{13}C{^{1}H} NMR spectrum of 1,2,3,4,5-pentaphenylbismole **5**.

Figure S12: ^{1}H NMR spectrum of 1-mesityl-2,3,4,5-tetraphenylbismole **6**.

Figure S13: Zoom in view of the ^{1}H NMR spectrum of 1-mesityl-2,3,4,5-tetraphenylbismole **6**.

Figure S14: $^{13}C\{^{1}H\}$ NMR spectrum of 1-mesityl-2,3,4,5-tetraphenylbismole **6**.

Figure S15: Zoomed in view of the $^{13}C\{^{1}H\}$ NMR spectrum of 1-mesityl-2,3,4,5-tetraphenylbismole **6**.

Figure S16: ^{1}H NMR spectrum of **7**.

Figure S17: $^{13}C\{^{1}H\}$ NMR spectrum of **7**.

Figure S18: Zoomed in view of the $^{13}C\{^{1}H\}$ NMR spectrum of **7**.

Figure S19: $^{11}B\{^{1}H\}$ NMR spectrum of **7**.

Figure S20: ^{1}H NMR spectrum of **8**.

Figure S21: $^{13}C\{^{1}H\}$ NMR spectrum of **8**.

Figure S22: $^{11}B\{^{1}H\}$ NMR spectrum of **8**.

Figure S23: Bismoles **1**-**8** in frozen 2-methyltetrahydrofuran at 77 K excited at 365 nm.

Figure S24: TIPL spectra of **4** at low temperature.

Figure S25: TRPL of **4** at low temperature.

Figure S26: TIPL spectra of **8** at 77 K over time.

Figure S27: TRPL-µs of **8** at low temperature.

Figure S28. Calculated UV-vis spectra of **4** (a), **7** (b) and **8** (c) at the B3LYP/cc-pVTZ(-PP) level of theory including the six singlet excitation states with the highest oscillator strength (given as red bars).

Figure S29. Calculated singlet and triplet states of **4** (a), **7** (b) and **8** (c) at the B3LYP/cc-pVTZ(-PP) level of theory. Oscillator strengths are indicated as follows: $f \geq 0.1$ (straight); $0.1 > f \geq 0.01$ (dashed); $0.01 > f \geq 0.001$ (dotted).

Figure S30. HOMO and LUMO of bismole **4**. MOs are calculated at the B3LYP/cc-pVTZ(-PP) level of theory and applying an *iso*-surface value of +0.02/–0.02 (red/green).

Figure S31. HOMO and LUMO of bismole **7**. MOs are calculated at the B3LYP/cc-pVTZ(-PP) level of theory applying an *iso*-surface value of +0.02/–0.02 (red/green).

Figure S32. HOMO and LUMO of bismole **8**. MOs are calculated at the B3LYP/cc-pVTZ(-PP) level of theory applying an *iso*-surface value of +0.02/–0.02 (red/green).

Figure S33. AIM bond paths motifs of bismole **7**.

Figure S34. a) *Iso*-surface representation of the localization domains of the ELI-D (Y = 1.4) of **7**. The basins are color coded from green (small) to blue (large); b) NCI *iso*-surfaces (s(**r**) = 0.5; attractive/repulsive non-covalent bonding aspects given in blue/red).

Figure S35. a) *Iso*-surface representation of the localization domains of the ELI-D (Y = 1.4) of **8**. The basins are color coded from green (small) to blue (large); b) NCI *iso*-surfaces (s(**r**) = 0.5; attractive/repulsive non-covalent bonding aspects given in blue/red).

Table S1: Crystallographic Experimental Details for **3**.

Table S2: Crystallographic Experimental Details for **4**.

Table S3: Crystallographic Experimental Details for **5**.

Table S4: Crystallographic Experimental Details for **6**.

Table S5: Crystallographic Experimental Details for **8**.

Table S6. TD-DFT calculated excited states of bismoles **4**, **7** and **8** at the B3LYP/cc-pVTZ(-PP) level of theory.

Table S7. TD-DFT calculated excited states of bismole **4** at B3LYP/TZ2P incl. SO coupling.

Table S8. TD-DFT calculated excited states of bismole **7** at B3LYP/TZ2P incl. SO coupling.

Table S9. TD-DFT calculated excited states of bismole **8** at B3LYP/TZ2P incl. SO coupling.

Table S10. Calculated vertical, adiabatic and zero-point energies of **4**, **7** and **8**.

Table S11. Topological real space bonding indicators derived from the computed electron density of relevant bcps in bismole **7** and **8**.

Table S12. ELI-D basin properties of bismole **7** and **8**.

Table S13. AIM atomic charges and Wiberg Bond-Indices derived from NBO analysis of **8** and **9**.

NMR Spectra

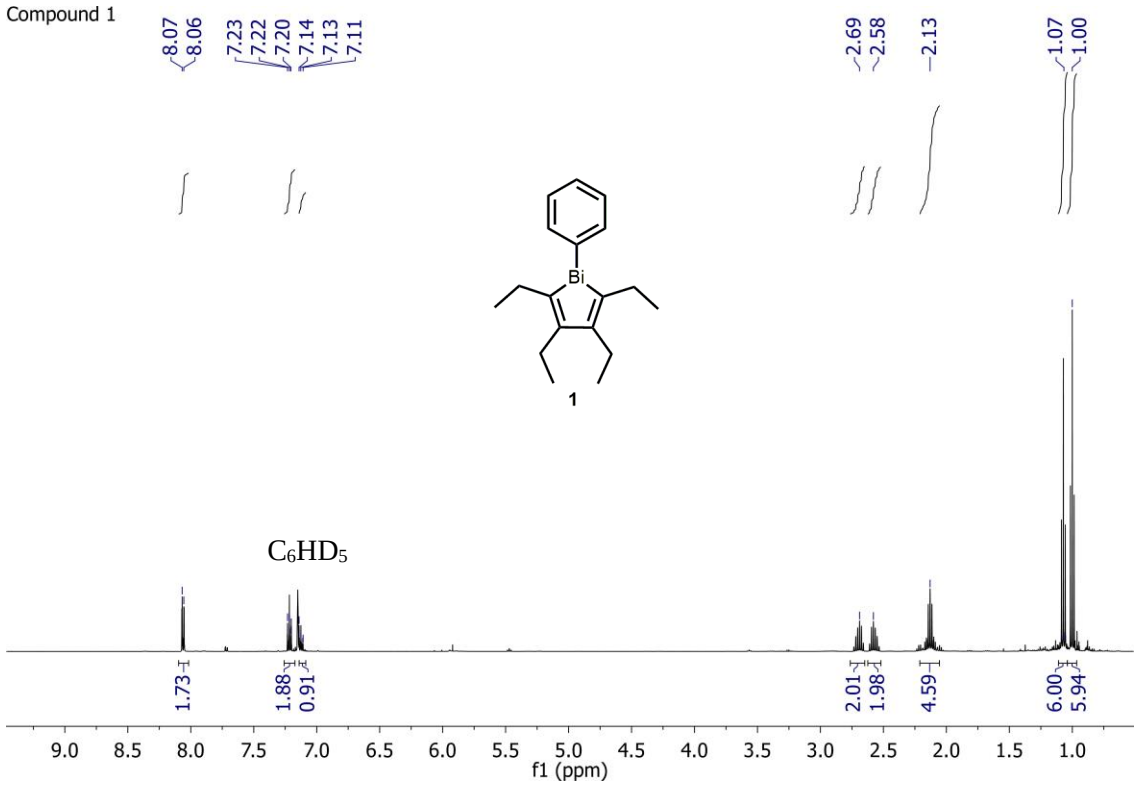


Figure S1. ^{1}H NMR spectrum of 1-phenyl-2,3,4,5-tetraethylbismole **1**.

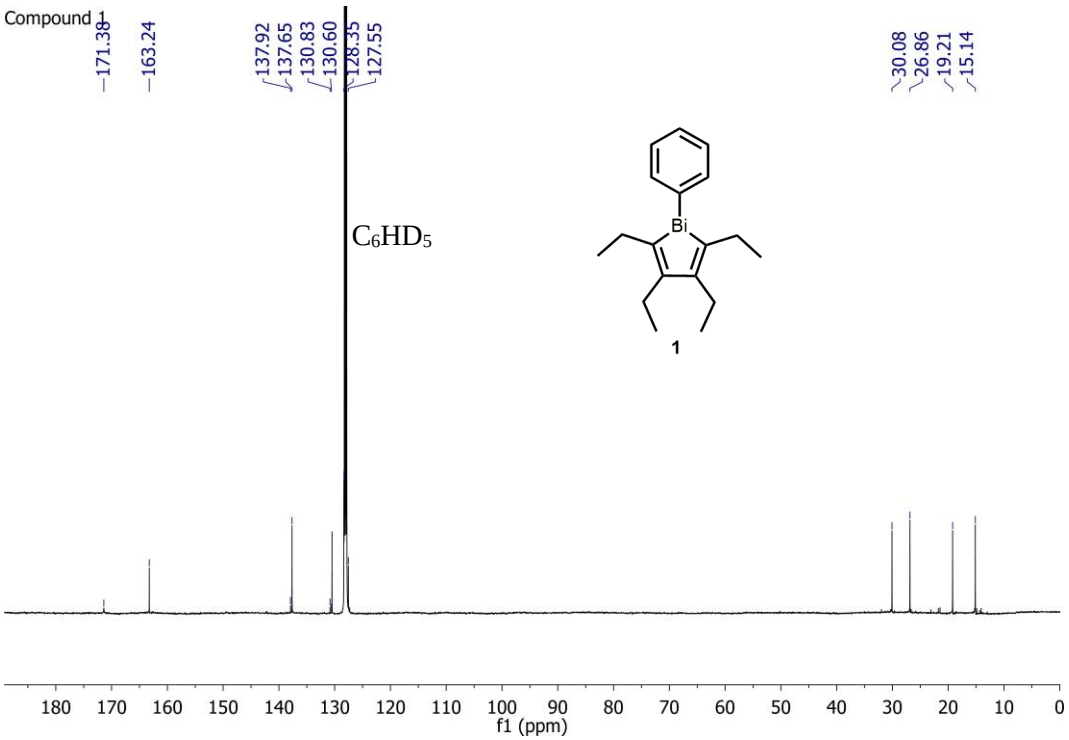


Figure S2. ^{13}C {^{1}H} NMR spectrum of 1-phenyl-2,3,4,5-tetraethylbismole **1**.

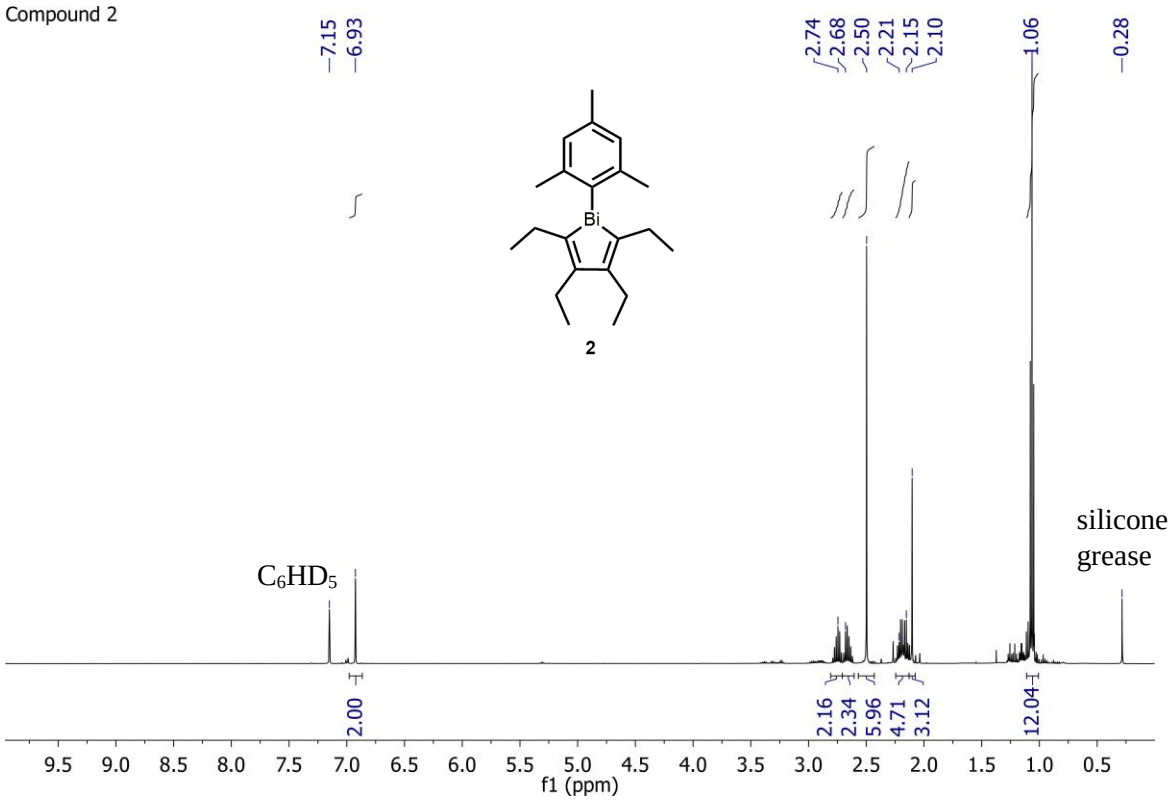


Figure S3. ^{1}H NMR spectrum of 1-mesityl-2,3,4,5-tetraethylbismole **2**.

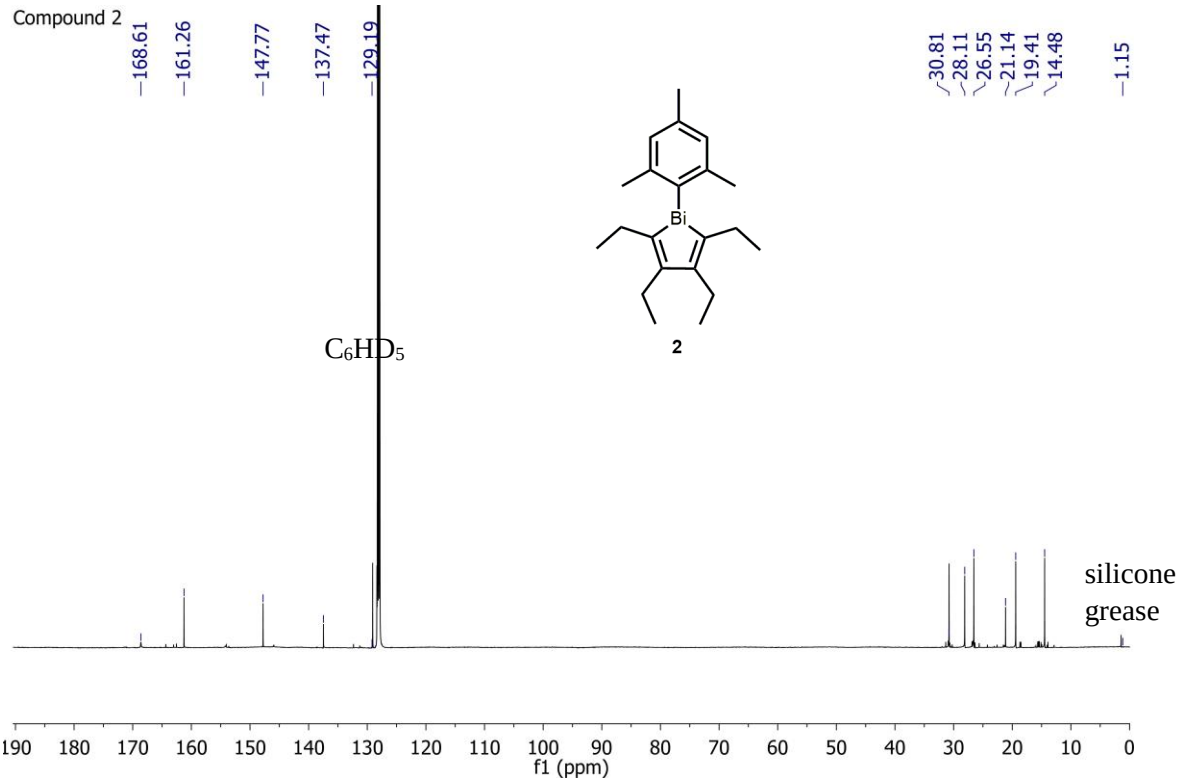


Figure S4. ^{13}C{^{1}H} NMR spectrum of 1-mesityl-2,3,4,5-tetraethylbismole **2**.

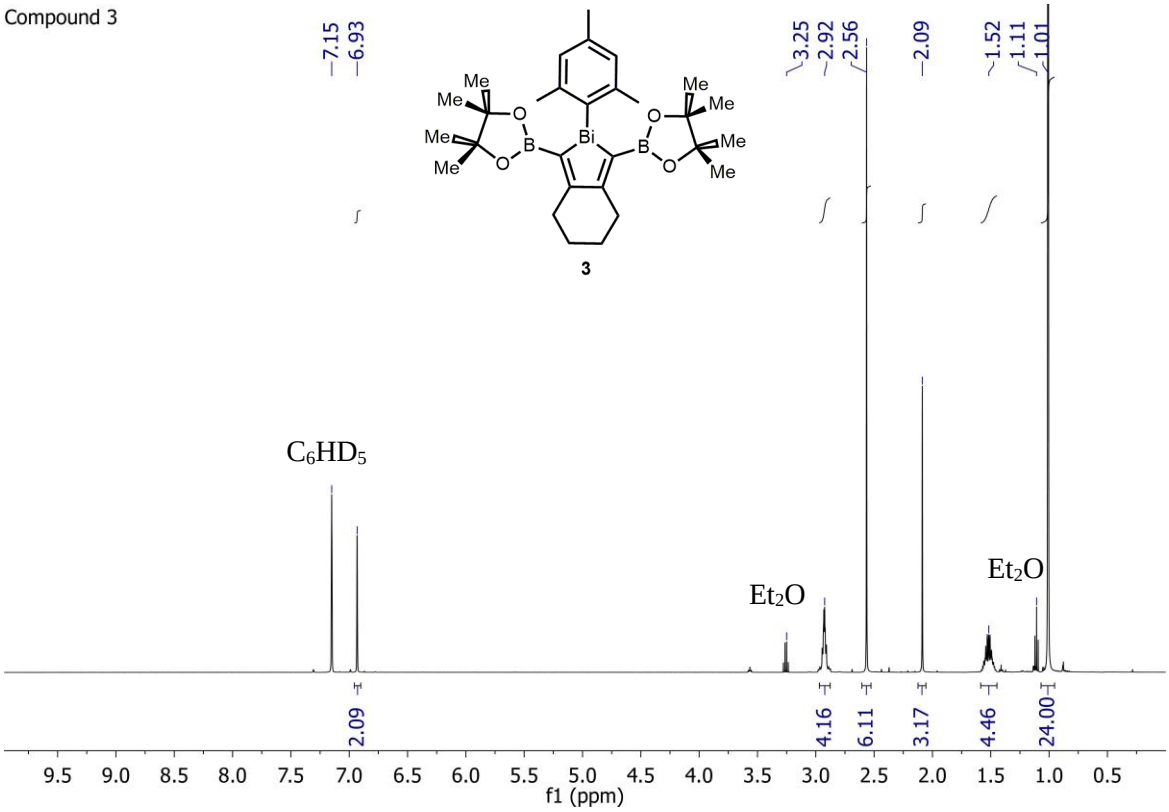


Figure S5. ^{1}H NMR spectrum of compound **3**.

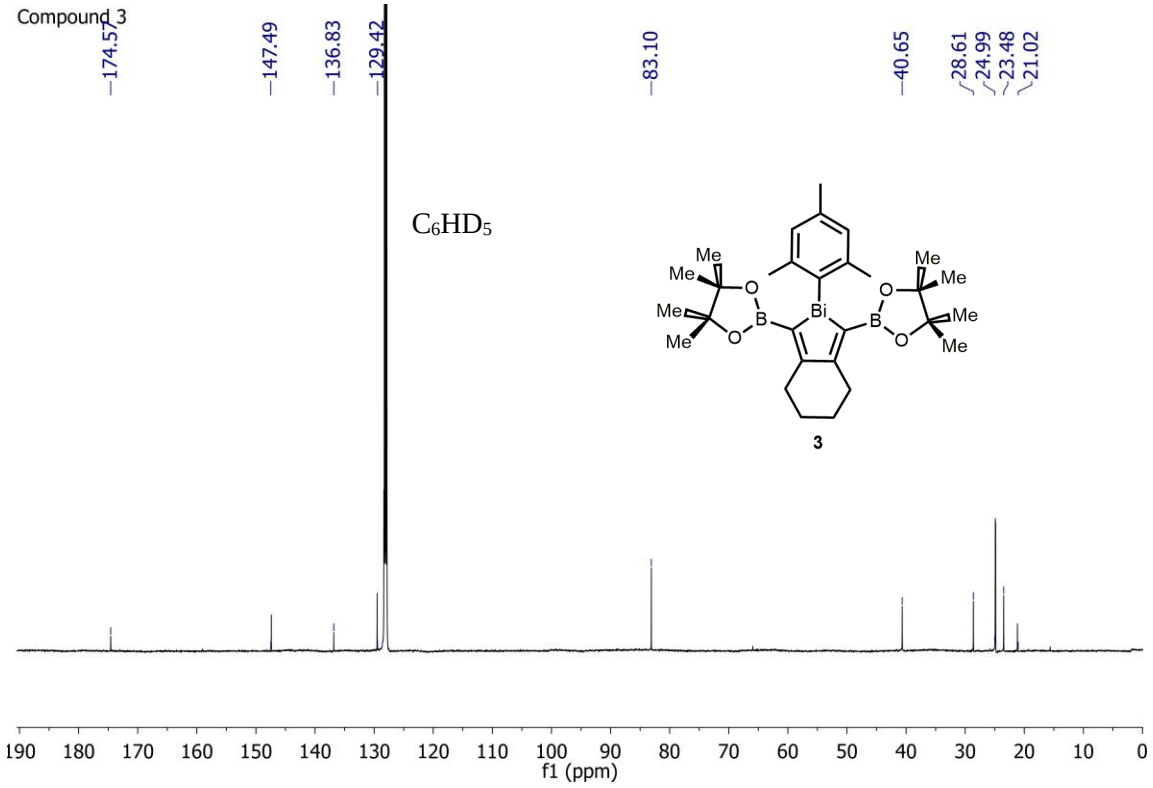


Figure S6. ^{13}C{^{1}H} NMR spectrum of compound **3**.

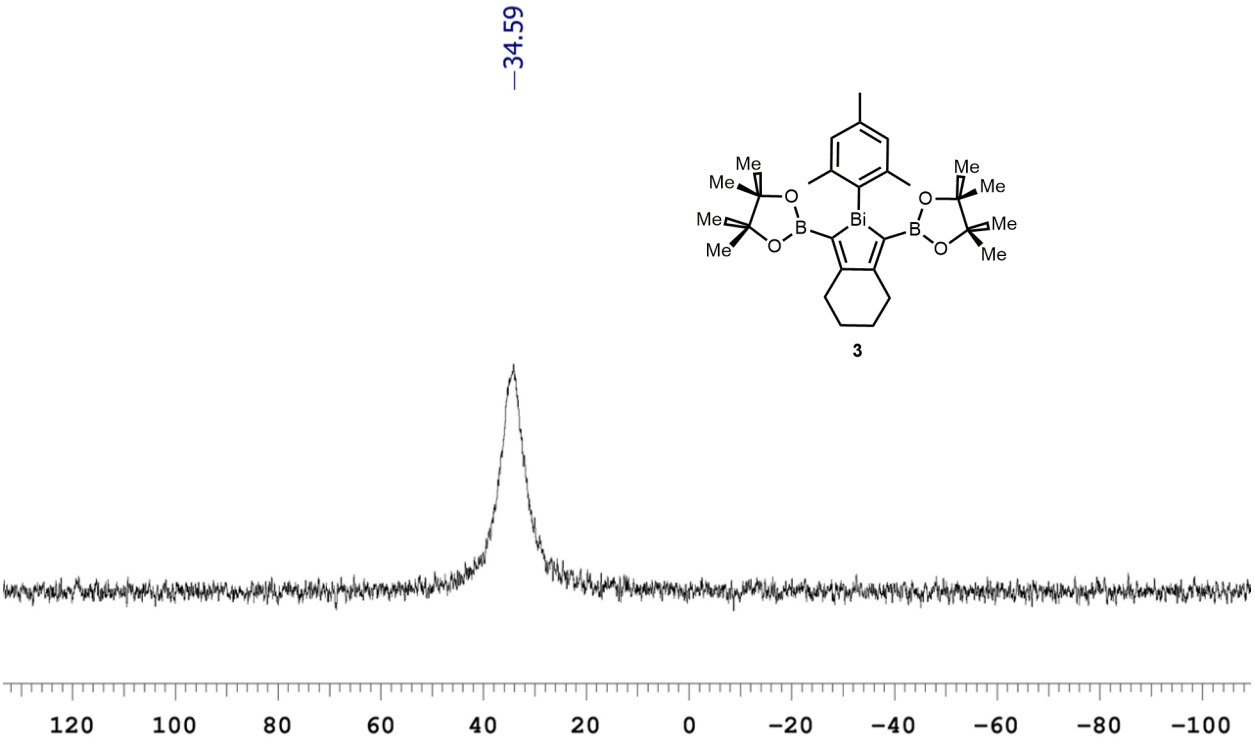


Figure S7. $^{11}B\{^{1}H\}$ NMR spectrum of compound **3**.

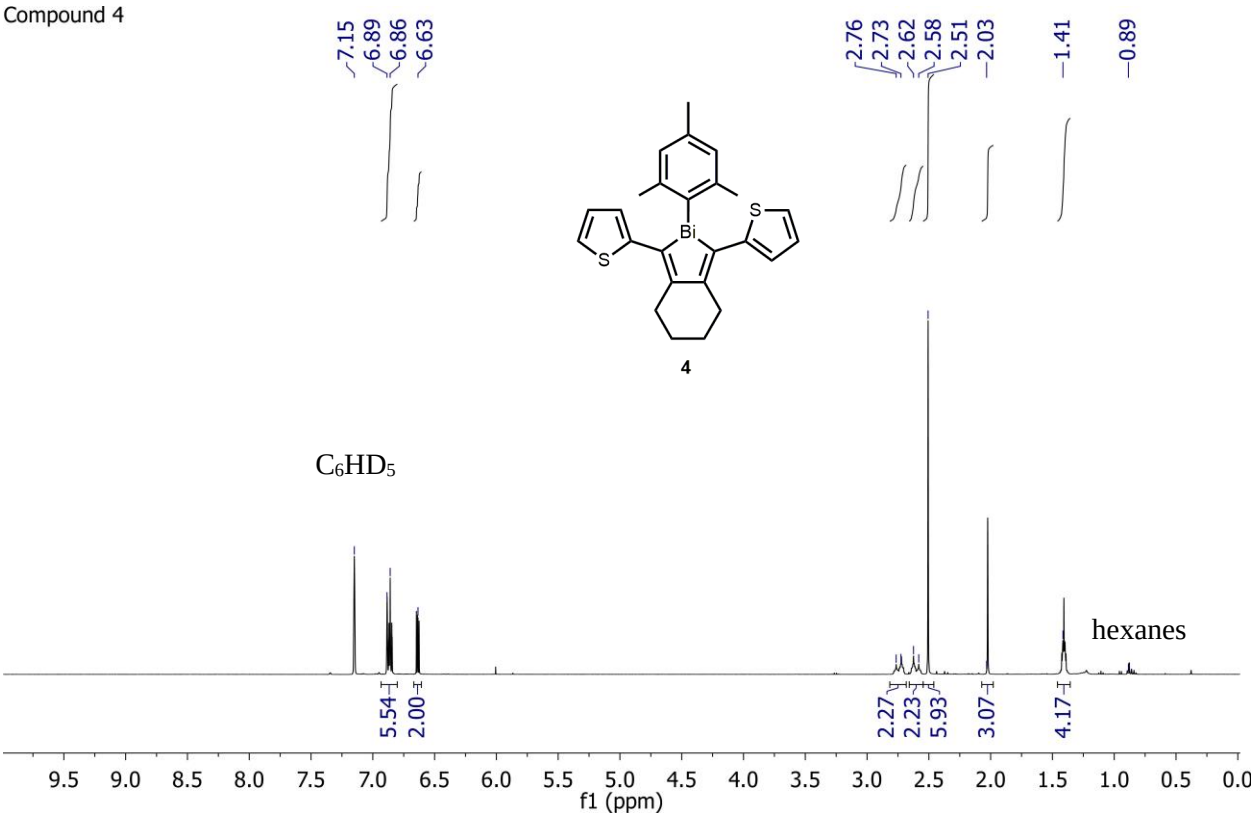


Figure S8. ^{1}H NMR spectrum of dithienyl bismole **4**.

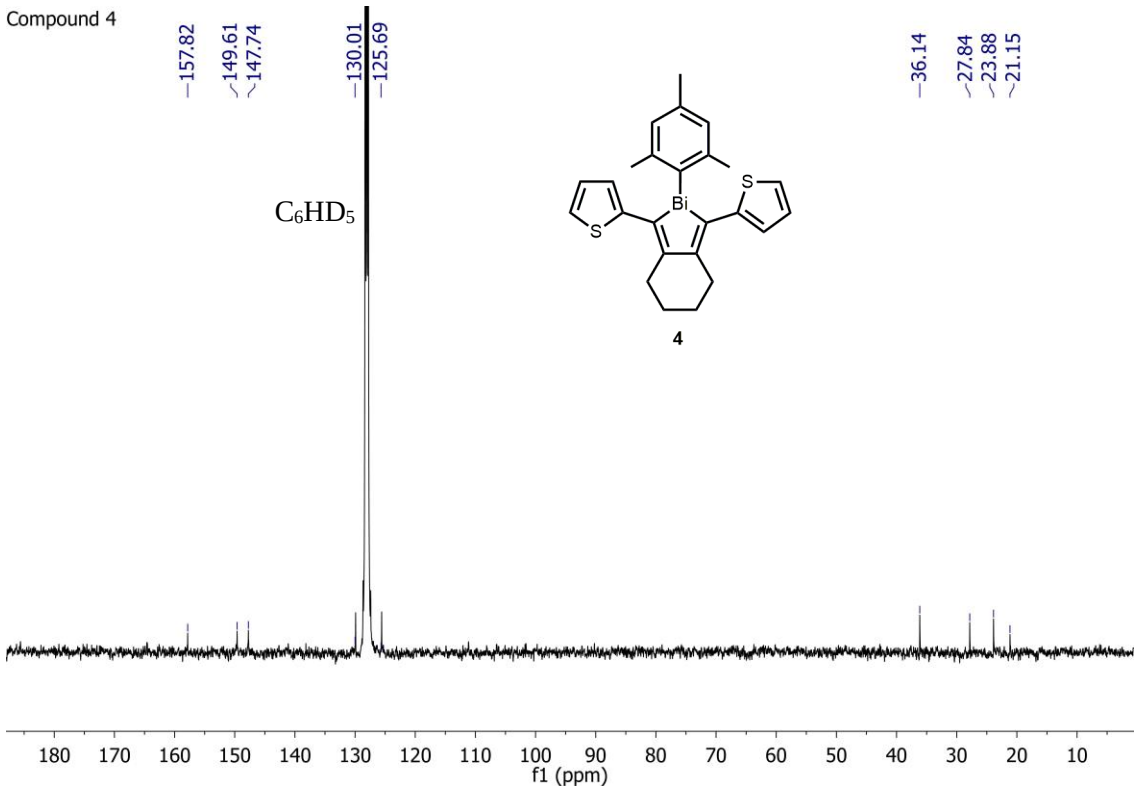


Figure S9. $^{13}C\{^{1}H\}$ NMR spectrum of dithienyl bismole **4**.

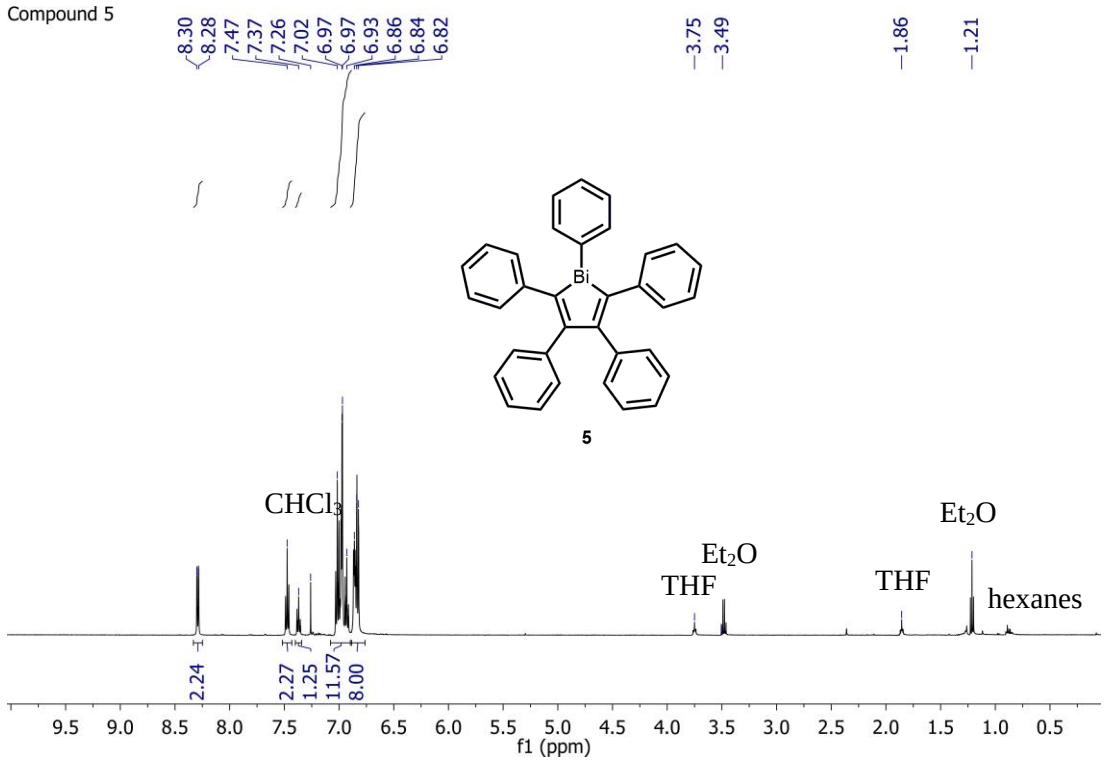


Figure S10. ^{1}H NMR spectrum of 1,2,3,4,5-pentaphenylbismole **5**.

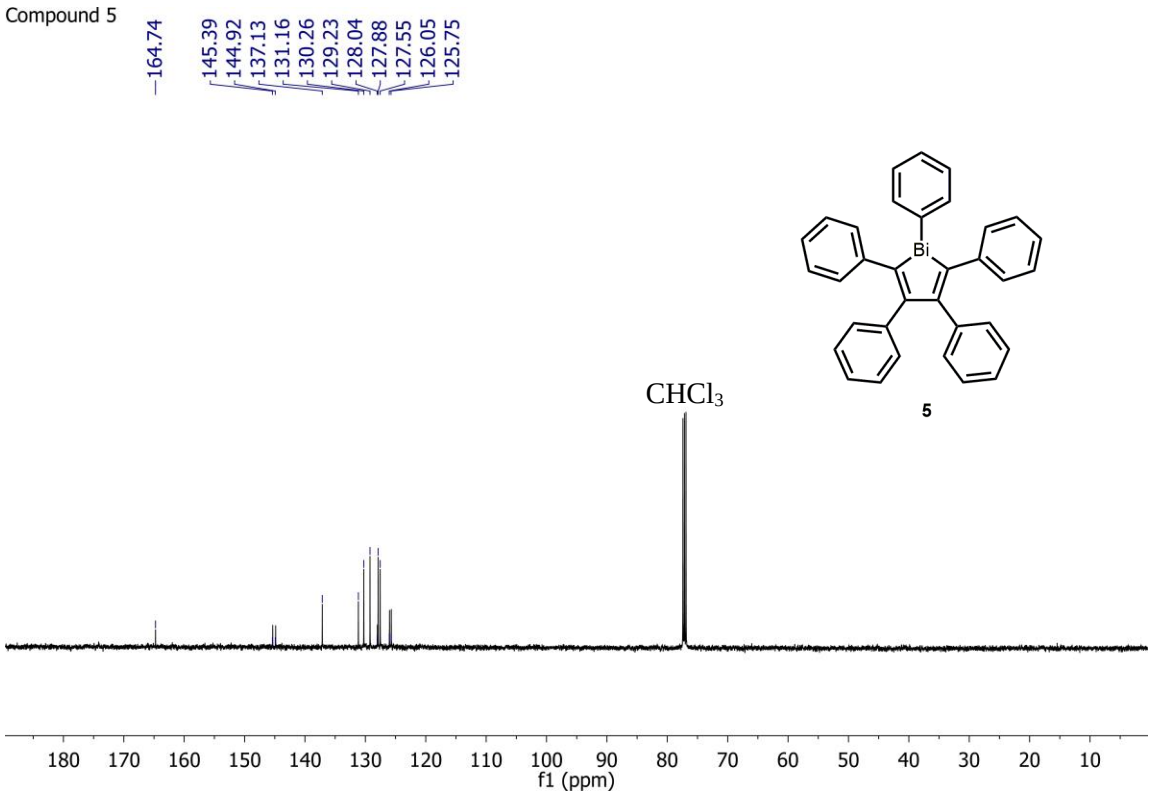


Figure S11. $^{13}C\{^{1}H\}$ NMR spectrum of 1,2,3,4,5-pentaphenylbismole **5**.

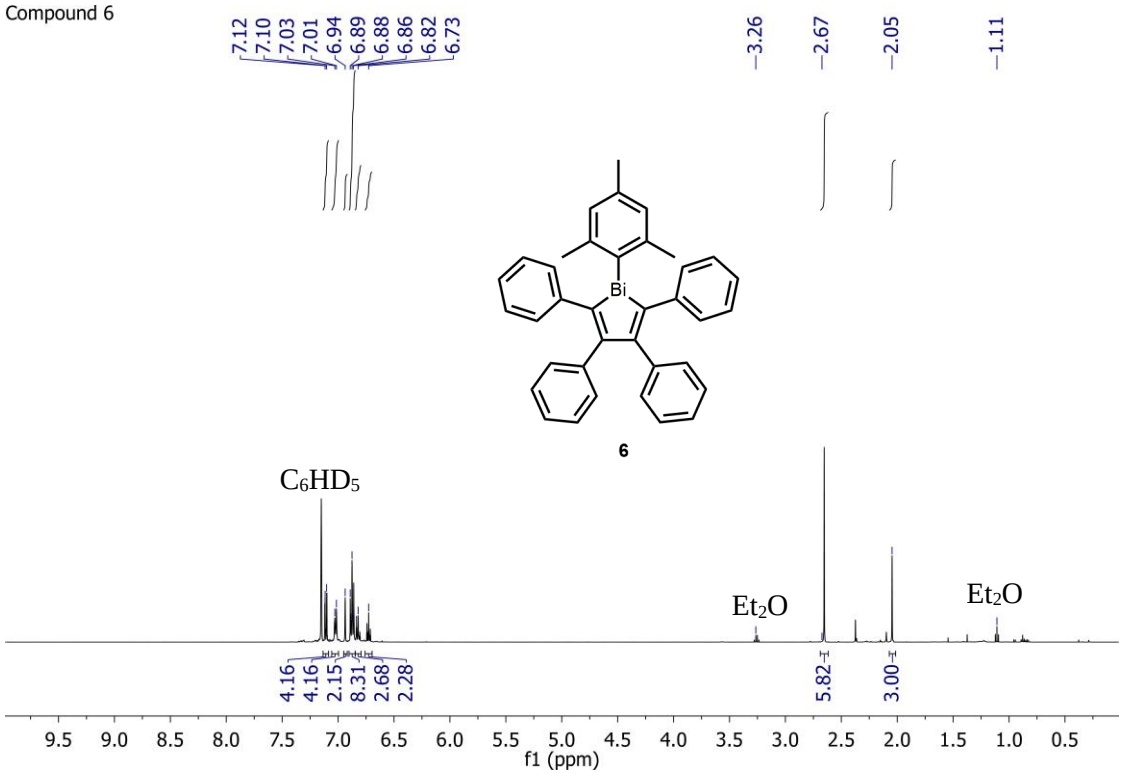


Figure S12. ^{1}H NMR spectrum of 1-mesityl-2,3,4,5-tetraphenylbismole **6**.

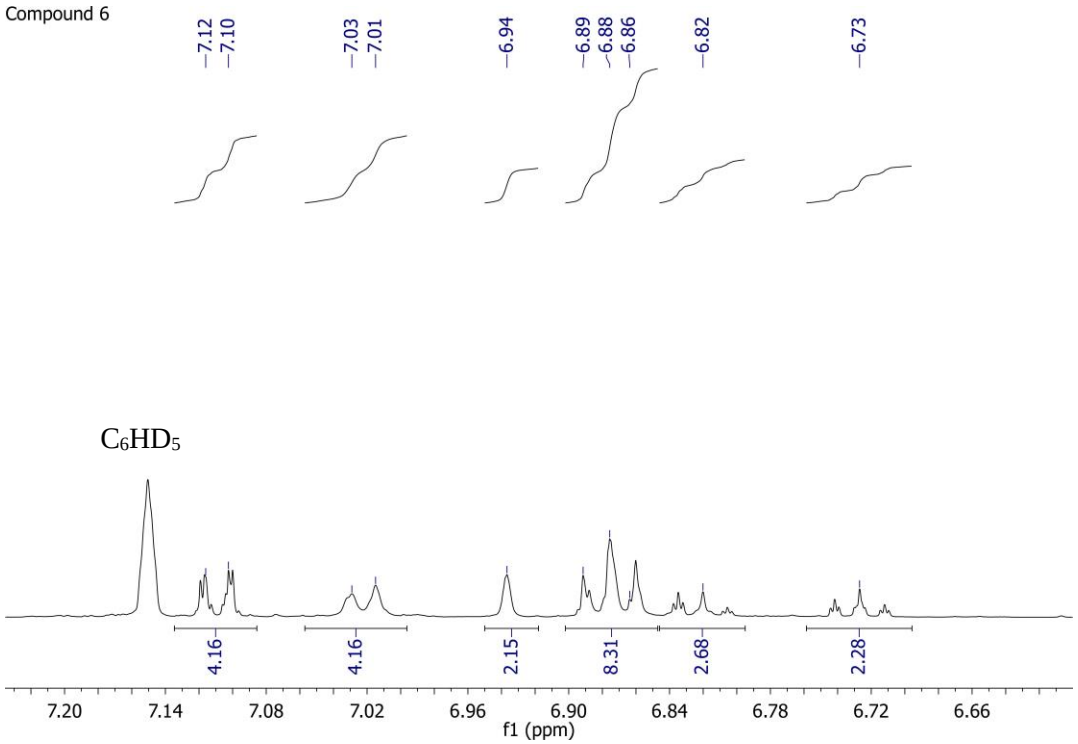


Figure S13. Zoom in view of the ^{1}H NMR spectrum of 1-mesityl-2,3,4,5-tetraphenylbismole **6**.

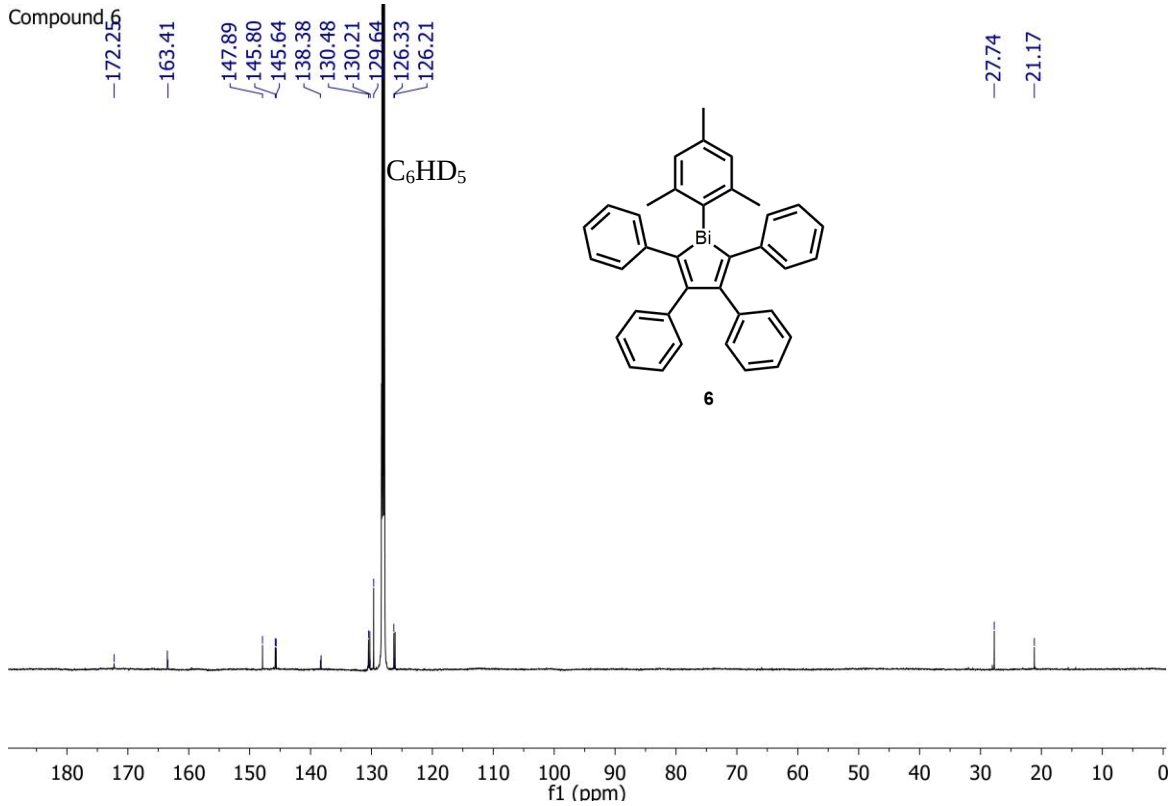


Figure S14. ^{13}C{^{1}H} NMR spectrum of 1-mesityl-2,3,4,5-tetraphenylbismole **6**.

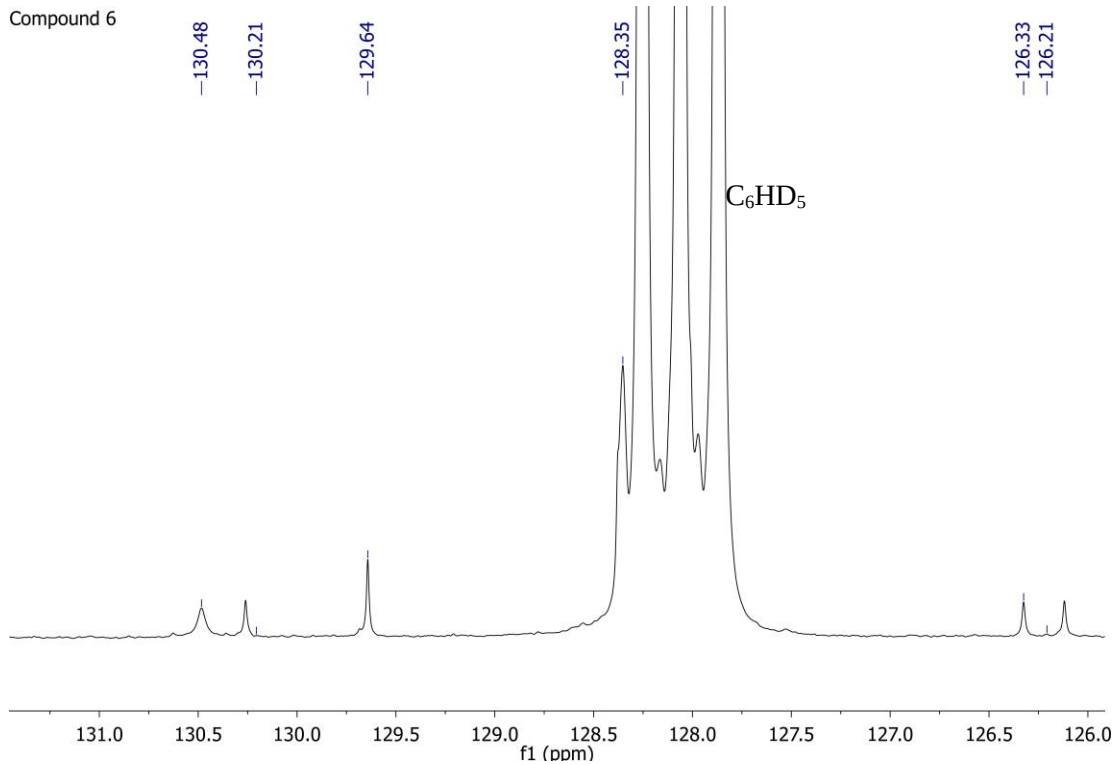


Figure S15. Zoomed in view of the $^{13}C\{^{1}H\}$ NMR spectrum of 1-mesityl-2,3,4,5-tetraphenylbismole **6**.

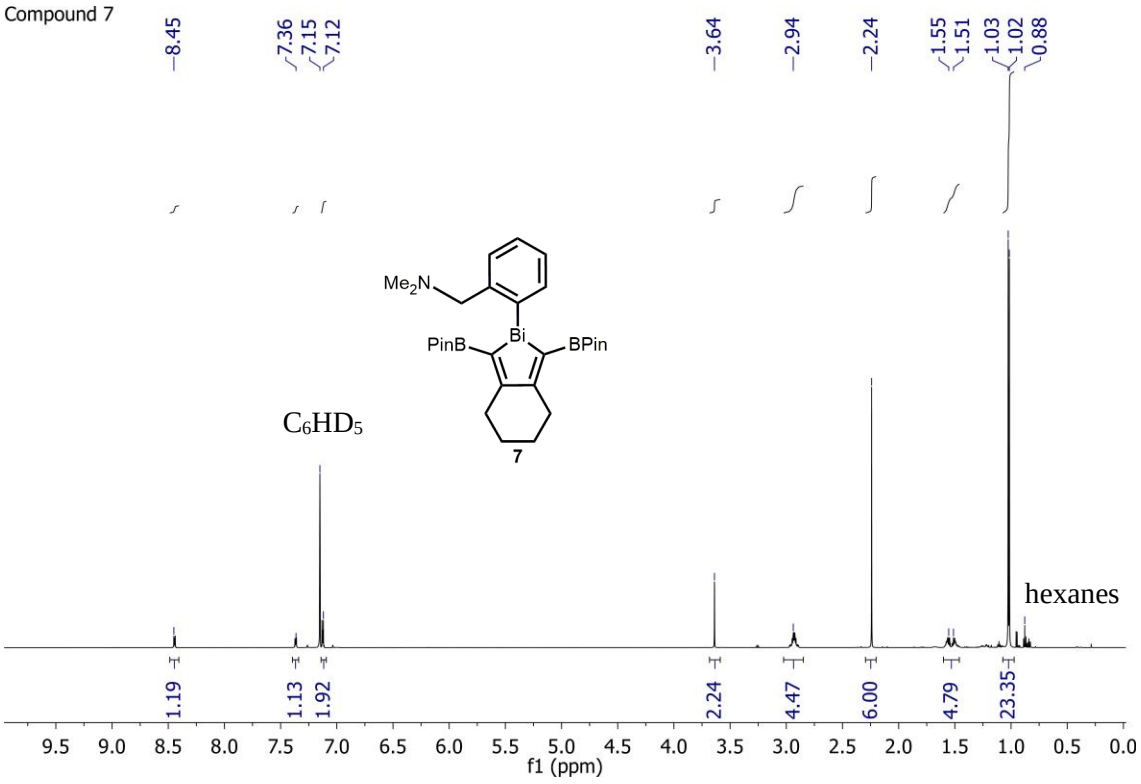


Figure S16. ^{1}H NMR spectrum of **7**.

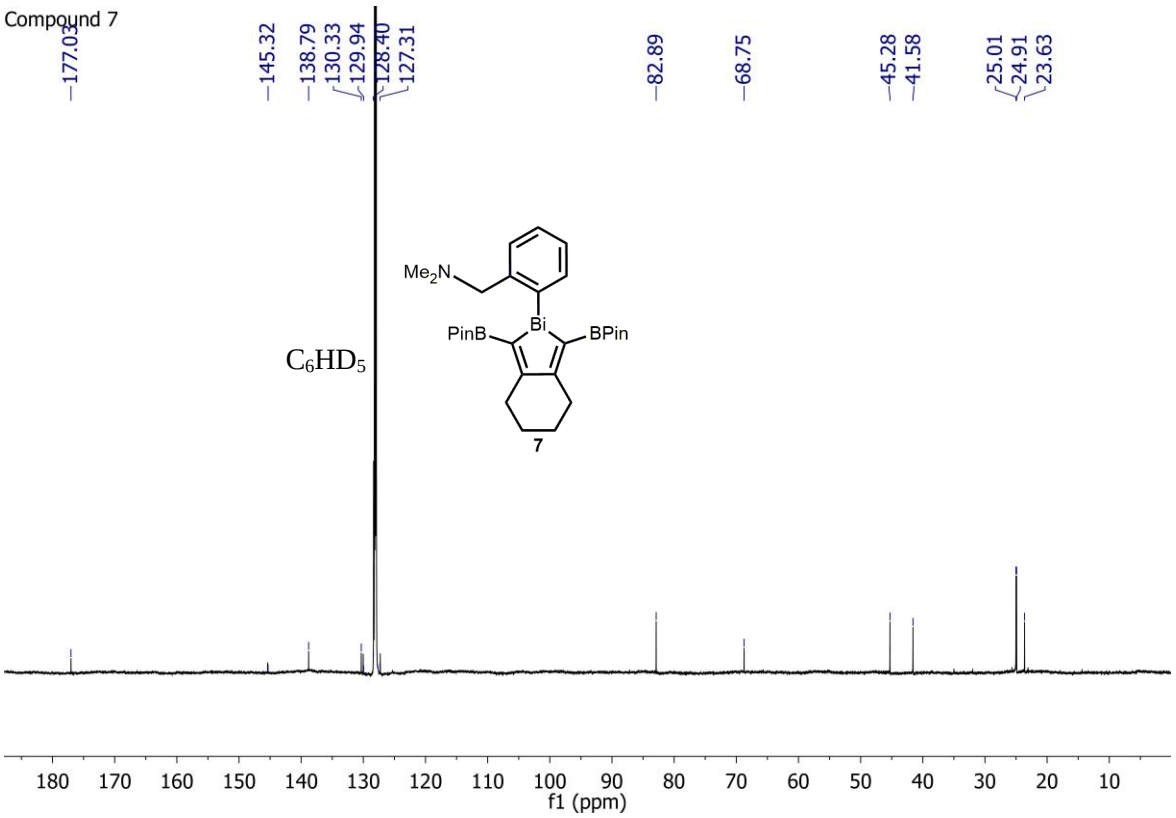


Figure S17. $^{13}C\{^{1}H\}$ NMR spectrum of **7**.

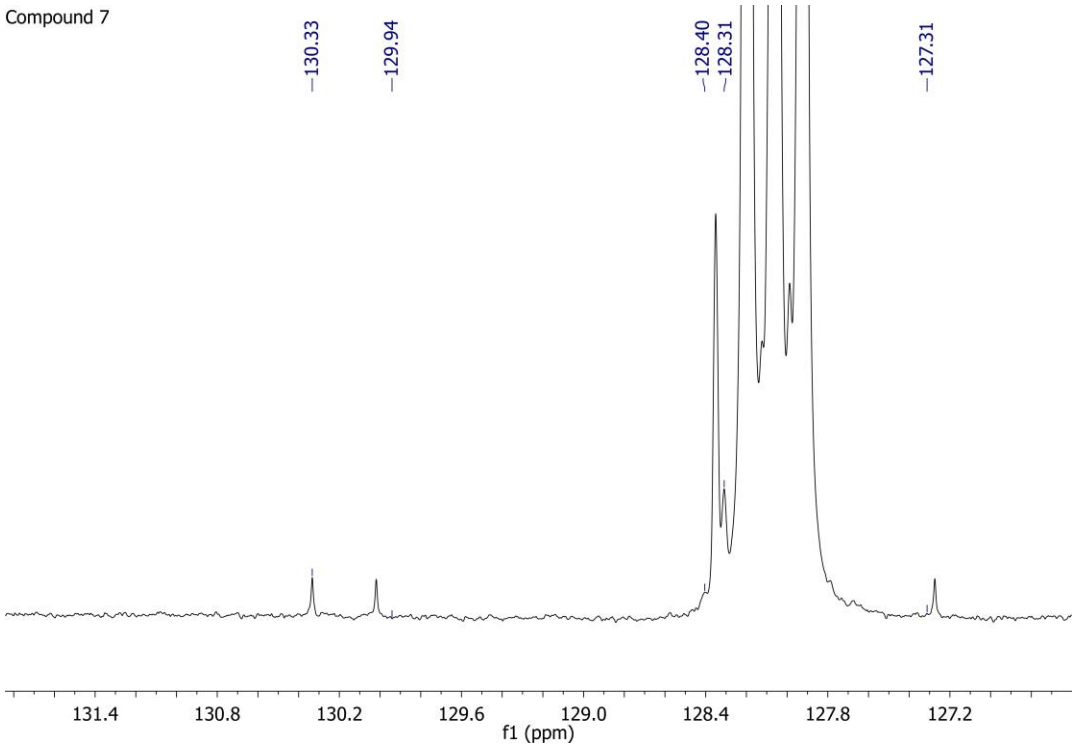


Figure S18. Zoomed in view of the $^{13}C\{^{1}H\}$ NMR spectrum of **7**.

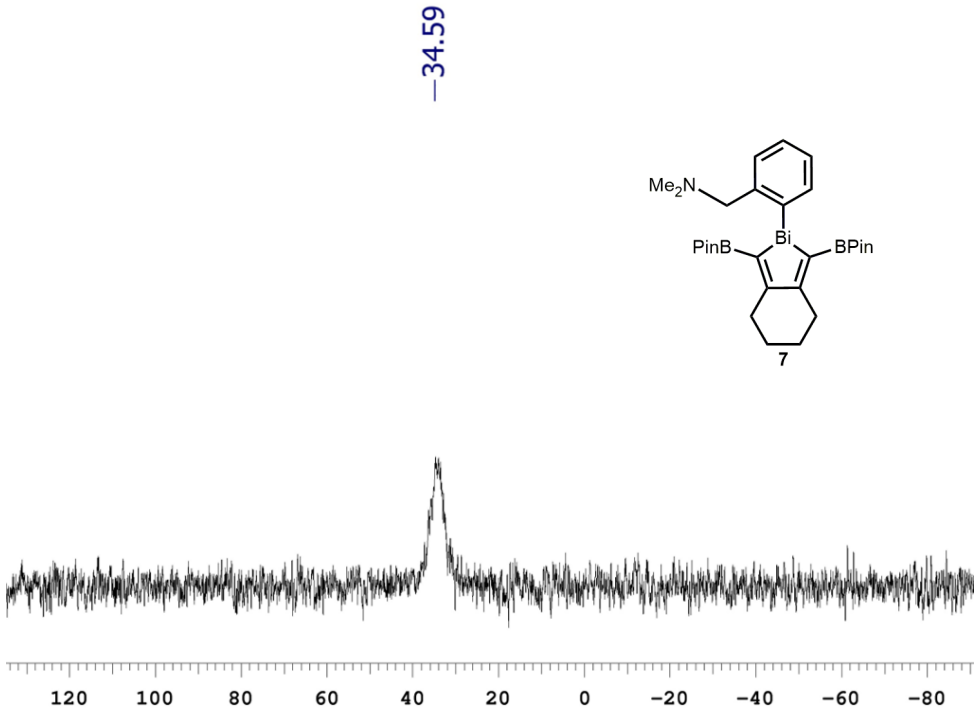


Figure S19. $^{11}B\{^{1}H\}$ NMR spectrum of **7**.

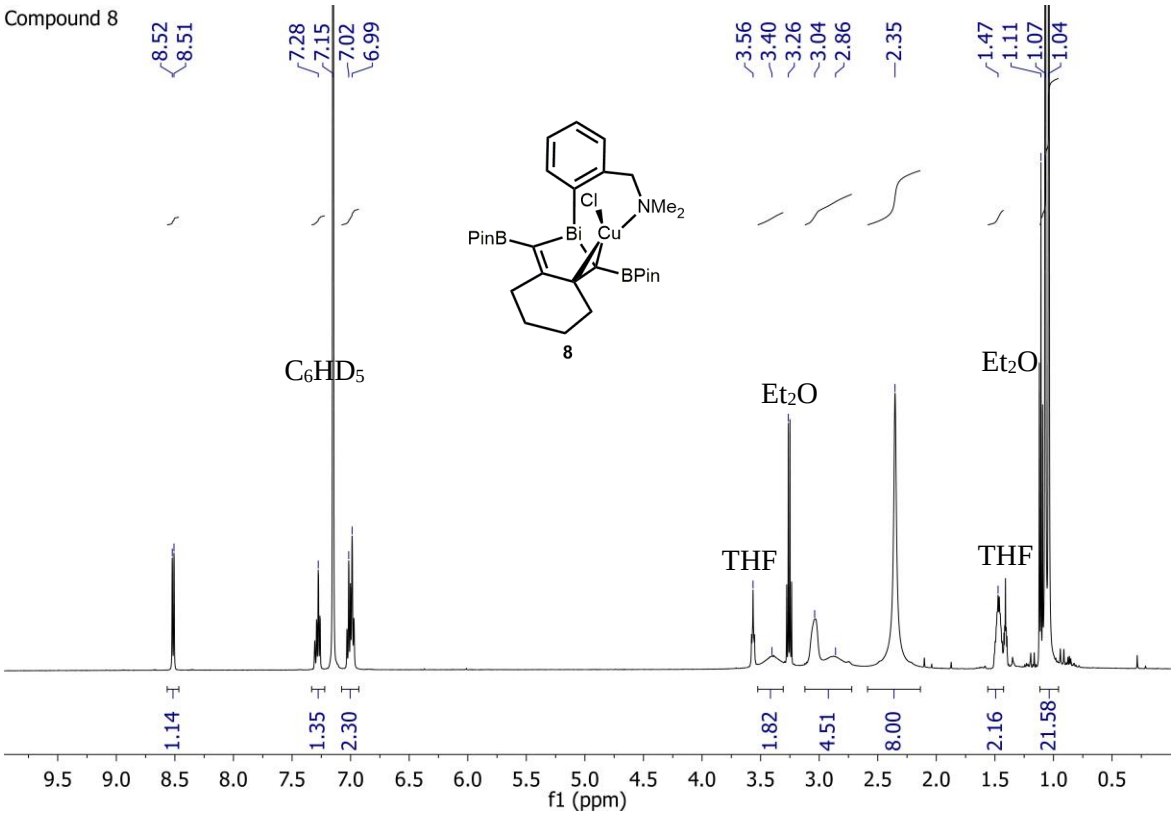


Figure S20. ^{1}H NMR spectrum of **8**.

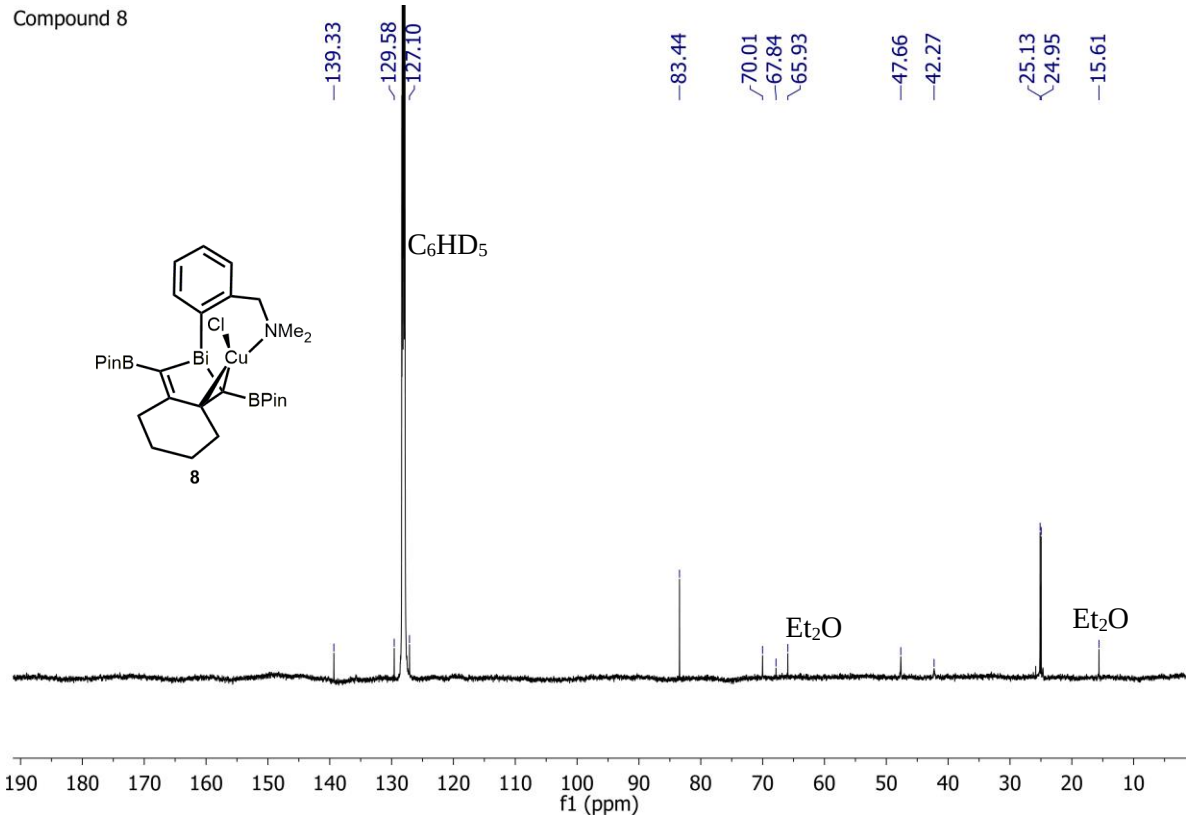


Figure S21. $^{13}C\{^{1}H\}$ NMR spectrum of **8**.

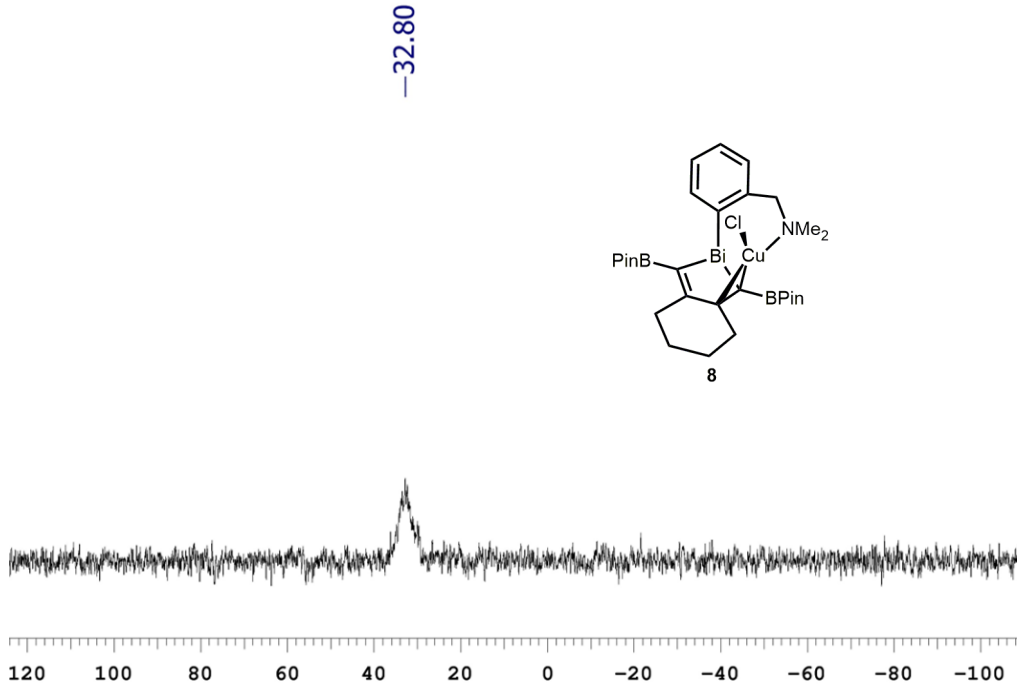


Figure S22. $^{11}B\{^{1}H\}$ NMR spectrum of **8**.

X-Ray Crystallographic Data

Table S1. Crystallographic Experimental Details for **3**.

A. Crystal Data	
formula	$C_{29}H_{43}B_2BiO_4$
formula weight	686.23
crystal dimensions (mm)	0.19 × 0.17 × 0.15
crystal system	monoclinic
space group	$P2_1/c$ (No. 14)
unit cell parameters[a]	
a (Å)	10.2343 (3)
b (Å)	15.8713 (5)
c (Å)	18.1272 (5)
β (deg)	95.4938 (9)
V (Å^3)	2930.91 (15)
Z	4
ρ_{calcd} (g cm^{-3})	1.555
μ (mm^{-1})	12.04
B. Data Collection and Refinement Conditions	
diffractometer	Bruker D8/APEX II CCD[b]
radiation (λ [Å])	Cu Kα (1.54178) (microfocus source)
temperature (°C)	–100
scan type	ω and ϕ scans (1.0°) (5 s exposures)
data collection 2θ limit (deg)	145.37
total data collected	19960 (-12 ≤ h ≤ 10, -19 ≤ k ≤ 19, -22 ≤ l ≤ 22)
independent reflections	5727 (R_{int} = 0.0209)
number of observed reflections (*NO*)	5605 [$F_o^2 \geq 2\sigma(F_o^2)$]
structure solution method	intrinsic phasing (*SHELXT-2013*[c])
refinement method	full-matrix least-squares on F^2 (*SHELXL–2013*[c])
absorption correction method	Gaussian integration (face-indexed)
range of transmission factors	0.3714–0.2154
data/restraints/parameters	5727 / 0 / 328
goodness-of-fit (S)[d] [all data]	1.099
final R indices[e]	
R_1 [$F_o^2 \geq 2\sigma(F_o^2)$]	0.0210
wR_2 [all data]	0.0536
largest difference peak and hole	1.021 and –0.689 e Å^{-3}

[a]Obtained from least-squares refinement of 9706 reflections with 7.42° < 2θ < 143.82°.

[b]Programs for diffractometer operation, data collection, data reduction and absorption correction were those supplied by Bruker.

(continued)

Table S1. Crystallographic Experimental Details (continued).

[c]Sheldrick, G. M. *Acta Crystallogr*. **2008**, *A64*, 112–122.

[d]$S = [\Sigma w(F_o^2 - F_c^2)^2/(n - p)]^{1/2}$ (n = number of data; p = number of parameters varied; $w = [\sigma^2(F_o^2) + (0.0235P)^2 + 4.2795P]^{-1}$ where $P = [\mathrm{Max}(F_o^2, 0) + 2F_c^2]/3$).

[e]$R_1 = \Sigma||F_o| - |F_c||/\Sigma|F_o|$; $wR_2 = [\Sigma w(F_o^2 - F_c^2)^2/\Sigma w(F_o^4)]^{1/2}$.

Table S2. Crystallographic Experimental Details for **4**.

A. Crystal Data	
formula	$C_{28}H_{28}BiS_2$
formula weight	637.60
crystal dimensions (mm)	0.38 × 0.24 × 0.05
crystal system	triclinic
space group	$P\bar{1}$ (No. 2)
unit cell parameters[a]	
a (Å)	9.1994 (4)
b (Å)	10.0707 (4)
c (Å)	13.8234 (6)
α (deg)	80.9431 (4)
β (deg)	80.1476 (4)
γ (deg)	75.9955 (4)
V (Å^3)	1215.22 (9)
Z	2
ρ_{calcd} (g cm^{-3})	1.743
μ (mm^{-1})	7.440
B. Data Collection and Refinement Conditions	
diffractometer	Bruker D8/APEX II CCD[b]
radiation (λ [Å])	graphite-monochromated Mo Kα (0.71073)
temperature (°C)	–100
scan type	ω scans (0.3°) (15 s exposures)
data collection 2θ limit (deg)	56.75
total data collected	11496 ($-12 \le h \le 12$, $-12 \le k \le 13$, $-18 \le l \le 18$)
independent reflections	5929 (R_{int} = 0.0122)
number of observed reflections (*NO*)	5604 [$F_o^2 \ge 2\sigma(F_o^2)$]
structure solution method	intrinsic phasing (*SHELXT-2014*[c])
refinement method	full-matrix least-squares on F^2 (*SHELXL–2014*[d])
absorption correction method	Gaussian integration (face-indexed)
range of transmission factors	0.7041–0.1417
data/restraints/parameters	5929 / 15[e] / 327
goodness-of-fit (*S*)[f] [all data]	1.084
final *R* indices[g]	
R_1 [$F_o^2 \ge 2\sigma(F_o^2)$]	0.0159
wR_2 [all data]	0.0364
largest difference peak and hole	0.907 and –0.658 e Å^{-3}

[a]Obtained from least-squares refinement of 9947 reflections with 4.60° < 2θ < 56.24°.

(continued)

Table S2. Crystallographic Experimental Details (continued).

[b]Programs for diffractometer operation, data collection, data reduction and absorption correction were those supplied by Bruker.

[c]Sheldrick, G. M. *Acta Crystallogr.* **2015**, *A71*, 3–8.

[d]Sheldrick, G. M. *Acta Crystallogr.* **2015**, *C71*, 3–8.

[e](a) The C4A–C5A and C4B–C5B distances were constrained to be equal (within 0.03 Å) during refinement. (b) The following distance restraints were applied to atoms of the minor-occupancy components of the disordered thien-2-yl groups: d(S1B–C11) = d(S1B–C14B) = d(S2B–C11) = d(S2B–C24B) = 1.71(1) Å; d(C11–C12B) = d(C12B–C13B) = d(C21–C22B) = d(C22B–C23B) = 1.43(1) Å, d(C13B–C14B) = d(C23B–C24B) = 1.35(1) Å. (c) The sets of atoms for the minor-occupancy components of the disordered thien-2-yl groups (i.e. {S1B, C11, C12B, C13B, C14B} and {S2B, C21, C22B, C23B, C24B}) were each constrained to be approximately planar by defining each five-atom set to comprise the vertices of a polyhedron with a volume of no more than 0.01 Å^3 (via the *SHELXL-2014* FLAT command).

[f]$S = [\Sigma w(F_o^2 - F_c^2)^2/(n-p)]^{1/2}$ (n = number of data; p = number of parameters varied; $w = [\sigma^2(F_o^2) + (0.0159P)^2 + 0.5123P]^{-1}$ where $P = [\mathrm{Max}(F_o^2, 0) + 2F_c^2]/3$).

[g]$R_1 = \Sigma||F_o| - |F_c||/\Sigma|F_o|$; $wR_2 = [\Sigma w(F_o^2 - F_c^2)^2/\Sigma w(F_o^4)]^{1/2}$.

Table S3. Crystallographic Experimental Details for **5**.

A. Crystal Data	
formula	$C_{34}H_{25}Bi$
formula weight	642.52
crystal dimensions (mm)	0.52 × 0.16 × 0.06
crystal system	monoclinic
space group	$P2_1$ (No. 4)
unit cell parameters[a]	
a (Å)	11.403 (3)
b (Å)	21.179 (5)
c (Å)	11.908 (3)
β (deg)	115.595 (2)
V (Å^3)	2593.6 (10)
Z	4
ρ_{calcd} (g cm^{-3})	1.645
μ (mm^{-1})	6.818
B. Data Collection and Refinement Conditions	
diffractometer	Bruker D8/APEX II CCD[b]
radiation (λ [Å])	graphite-monochromated Mo Kα (0.71073)
temperature (°C)	–100
scan type	ω scans (0.3°) (15 s exposures)
data collection 2θ limit (deg)	56.73
total data collected	24157 (-14 ≤ h ≤ 15, -27 ≤ k ≤ 28, -15 ≤ l ≤ 15)
independent reflections	12584 (R_{int} = 0.0245)
number of observed reflections (*NO*)	11786 [$F_o^2 \geq 2\sigma(F_o^2)$]
structure solution method	Patterson/structure expansion (*DIRDIF–2008*[c])
refinement method	full-matrix least-squares on F^2 (*SHELXL–2014*[d])
absorption correction method	Gaussian integration (face-indexed)
range of transmission factors	0.7253–0.1742
data/restraints/parameters	12584 / 0 / 632
Flack absolute structure parameter[e]	0.096(4)
goodness-of-fit (*S*)[f] [all data]	0.911
final *R* indices[g]	
R_1 [$F_o^2 \geq 2\sigma(F_o^2)$]	0.0192
wR_2 [all data]	0.0349
largest difference peak and hole	0.844 and –0.658 e Å^{-3}

[a]Obtained from least-squares refinement of 9908 reflections with 4.40° < 2θ < 48.34°.

[b]Programs for diffractometer operation, data collection, data reduction and absorption correction were those supplied by Bruker.

(continued)

Table S3. Crystallographic Experimental Details (continued).

[c]Beurskens, P. T.; Beurskens, G.; de Gelder, R.; Smits, J. M. M.; Garcia-Granda, S.; Gould, R. O. (2008). The *DIRDIF-2008* program system. Crystallography Laboratory, Radboud University Nijmegen, The Netherlands.

[d]Sheldrick, G. M. *Acta Crystallogr.* **2015**, *C71*, 3–8.

[e]Flack, H. D. *Acta Crystallogr.* **1983**, *A39*, 876–881; Flack, H. D.; Bernardinelli, G. *Acta Crystallogr.* **1999**, *A55*, 908–915; Flack, H. D.; Bernardinelli, G. *J. Appl. Cryst.* **2000**, *33*, 1143–1148. The Flack parameter will refine to a value near zero if the structure is in the correct configuration and will refine to a value near one for the inverted configuration. The value observed herein is indicative of a small degree of racemic twinning, and was accomodated during the refinement (using the *SHELXL-2014* TWIN instruction [see reference *d*]). The refined value of the Flack parameter (here, 0.096(4)) thus represents the approximate fraction of the minor twin component (i.e. the components are present in about a 90:10 ratio).

[f]$S = [\Sigma w(F_o^2 - F_c^2)^2/(n - p)]^{1/2}$ (n = number of data; p = number of parameters varied; $w = \sigma^2(F_o^2)$).

[g]$R_1 = \Sigma||F_o| - |F_c||/\Sigma|F_o|$; $wR_2 = [\Sigma w(F_o^2 - F_c^2)^2/\Sigma w(F_o^4)]^{1/2}$.

Table S4. Crystallographic Experimental Details for **6**.

A. Crystal Data	
formula	$C_{37}H_{31}Bi$
formula weight	684.60
crystal dimensions (mm)	0.21 × 0.19 × 0.05
crystal system	monoclinic
space group	$P2_1/c$ (No. 14)
unit cell parameters[a]	
a (Å)	16.3505 (4)
b (Å)	10.6036 (2)
c (Å)	18.0431 (4)
β (deg)	113.3156 (6)
V (Å^3)	2872.75 (11)
Z	4
ρ_{calcd} (g cm^{-3})	1.583
μ (mm^{-1})	12.20
B. Data Collection and Refinement Conditions	
diffractometer	Bruker D8/APEX II CCD[b]
radiation (λ [Å])	Cu Kα (1.54178) (microfocus source)
temperature (°C)	–100
scan type	ω and ϕ scans (1.0°) (5 s exposures)
data collection 2θ limit (deg)	147.90
total data collected	19998 (-20 ≤ h ≤ 19, -13 ≤ k ≤ 13, -22 ≤ l ≤ 22)
independent reflections	5811 (R_{int} = 0.0251)
number of observed reflections (*NO*)	5764 [$F_o^2 \geq 2\sigma(F_o^2)$]
structure solution method	intrinsic phasing (*SHELXT-2014*[c])
refinement method	full-matrix least-squares on F^2 (*SHELXL–2014*[d])
absorption correction method	Gaussian integration (face-indexed)
range of transmission factors	0.7345–0.2010
data/restraints/parameters	5811 / 0 / 346
goodness-of-fit (S)[e] [all data]	1.127
final R indices[f]	
R_1 [$F_o^2 \geq 2\sigma(F_o^2)$]	0.0198
wR_2 [all data]	0.0505
largest difference peak and hole	0.746 and –1.741 e Å^{-3}

[a]Obtained from least-squares refinement of 9973 reflections with 9.90° < 2θ < 147.24°.

[b]Programs for diffractometer operation, data collection, data reduction and absorption correction were those supplied by Bruker.

(continued)

Table S4. Crystallographic Experimental Details (continued).

[c]Sheldrick, G. M. *Acta Crystallogr.* **2015**, *A71*, 3–8. (*SHELXT-2014*)

[d]Sheldrick, G. M. *Acta Crystallogr.* **2015**, *C71*, 3–8. (*SHELXL-2014*)

[e]$S = [\Sigma w(F_o^2 - F_c^2)^2/(n - p)]^{1/2}$ (n = number of data; p = number of parameters varied; $w = [\sigma^2(F_o^2) + (0.0241P)^2 + 2.9401P]^{-1}$ where $P = [\mathrm{Max}(F_o^2, 0) + 2F_c^2]/3$).

[f]$R_1 = \Sigma||F_o| - |F_c||/\Sigma|F_o|$; $wR_2 = [\Sigma w(F_o^2 - F_c^2)^2/\Sigma w(F_o^4)]^{1/2}$.

Table S5. Crystallographic Experimental Details for **8**.

A. Crystal Data	
formula	$C_{31}H_{49}B_2BiClCuNO_{4.5}$
formula weight	837.30
crystal dimensions (mm)	0.17 × 0.16 × 0.06
crystal system	monoclinic
space group	$P2_1/n$ (an alternate setting of $P2_1/c$ [No. 14])
unit cell parameters[a]	
a (Å)	10.9507 (3)
b (Å)	11.6200 (4)
c (Å)	27.0561 (8)
β (deg)	94.8831 (4)
V (Å^3)	3430.31 (18)
Z	4
ρ_{calcd} (g cm^{-3})	1.621
μ (mm^{-1})	5.857
B. Data Collection and Refinement Conditions	
diffractometer	Bruker D8/APEX II CCD[b]
radiation (λ [Å])	graphite-monochromated Mo Kα (0.71073)
temperature (°C)	–100
scan type	ω scans (0.3°) (15 s exposures)
data collection 2θ limit (deg)	56.67
total data collected	31526 (-14 ≤ h ≤ 14, -15 ≤ k ≤ 15, -36 ≤ l ≤ 35)
independent reflections	8483 (R_{int} = 0.0406)
number of observed reflections (*NO*)	7009 [$F_o^2 \geq 2\sigma(F_o^2)$]
structure solution method	Patterson/structure expansion (*DIRDIF–2008*[c])
refinement method	full-matrix least-squares on F^2 (*SHELXL–2014*[d,e])
absorption correction method	Gaussian integration (face-indexed)
range of transmission factors	0.7621–0.4998
data/restraints/parameters	8483 / 7[f] / 432
goodness-of-fit (S)[g] [all data]	1.018
final R indices[h]	
R_1 [$F_o^2 \geq 2\sigma(F_o^2)$]	0.0257
wR_2 [all data]	0.0609
largest difference peak and hole	1.667 and –0.611 e Å^{-3}

[a]Obtained from least-squares refinement of 9914 reflections with 4.62° < 2θ < 45.64°.

[b]Programs for diffractometer operation, data collection, data reduction and absorption correction were those supplied by Bruker.

(continued)

Table S5. Crystallographic Experimental Details (continued).

[c]Beurskens, P. T.; Beurskens, G.; de Gelder, R.; Smits, J. M. M.; Garcia-Granda, S.; Gould, R. O. (2008). The *DIRDIF-2008* program system. Crystallography Laboratory, Radboud University Nijmegen, The Netherlands.

[d]Sheldrick, G. M. *Acta Crystallogr.* **2015**, *C71*, 3–8.

[e]Attempts to refine peaks of residual electron density as disordered or partial-occupancy solvent diethyl ether oxygen or carbon atoms were unsuccessful. The data were corrected for disordered electron density through use of the SQUEEZE procedure as implemented in *PLATON* (Spek, A. L. *Acta Crystallogr.* **2015**, *C71*, 9–18. *PLATON* - a multipurpose crystallographic tool. Utrecht University, Utrecht, The Netherlands). A total solvent-accessible void volume of 303.0 Å^3 with a total electron count of 74 (consistent with 2 molecules of solvent diethyl ether, or 0.5 molecules per formula unit of the bismole-copper complex molecule) was found in the unit cell.

[f](a) The C11A–C12A and C11B–C12B distances were constrained to be equal (within 0.03 Å) during refinement. (b) The following distances were constrained to be equal to idealized values during refinement: d(C11B–C13B) = d(C11B–C14B) = d(C12B–C15B) = d(C12B–C16B) = 1.52(1) Å; d(C13B...C14B) = d(C15B...C16B) = 2.48(1) Å.

[g]$S = [\Sigma w(F_o^2 - F_c^2)^2/(n - p)]^{1/2}$ (n = number of data; p = number of parameters varied; $w = [\sigma^2(F_o^2) + (0.0291P)^2 + 0.4810P]^{-1}$ where $P = [\mathrm{Max}(F_o^2, 0) + 2F_c^2]/3$).

[h]$R_1 = \Sigma||F_o| - |F_c||/\Sigma|F_o|$; $wR_2 = [\Sigma w(F_o^2 - F_c^2)^2/\Sigma w(F_o^4)]^{1/2}$.

Photoluminescence data

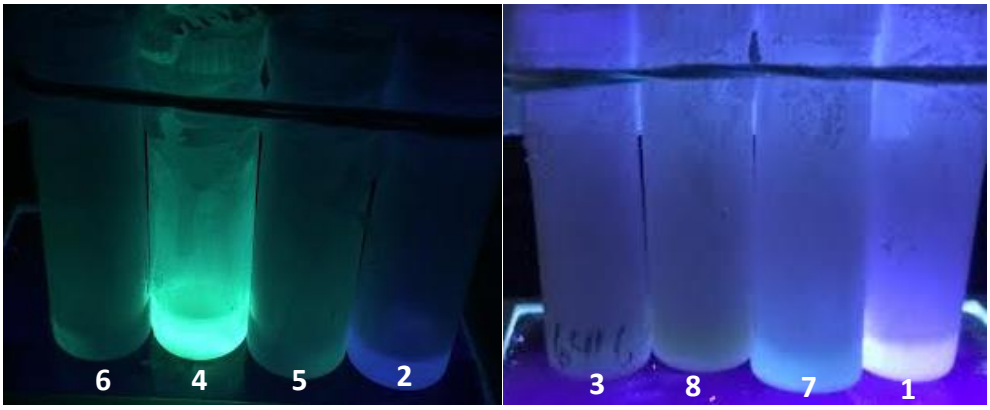


Figure S23. Bismoles **1-8** in frozen 2-methyltetrahydrofuran at 77 K excited at 365 nm.

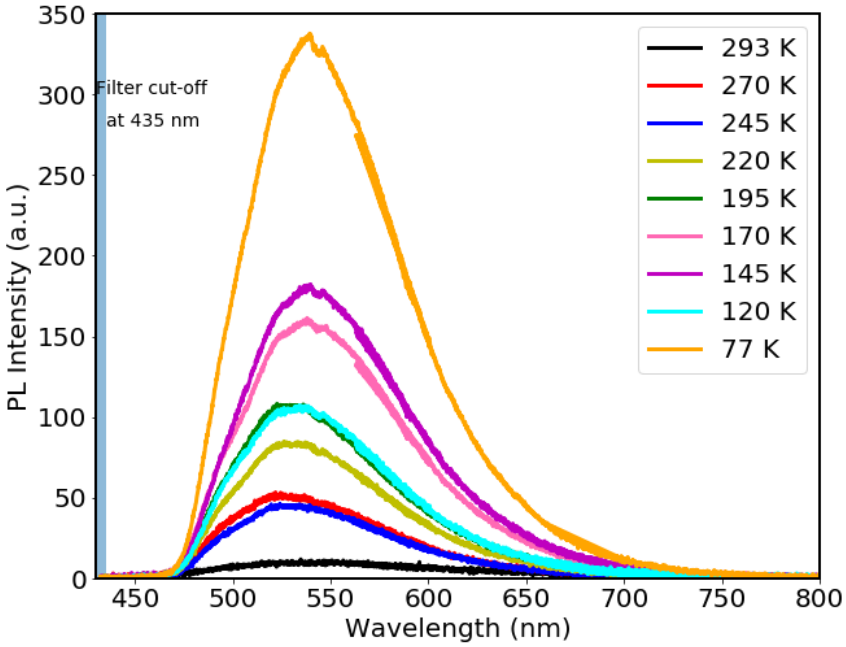
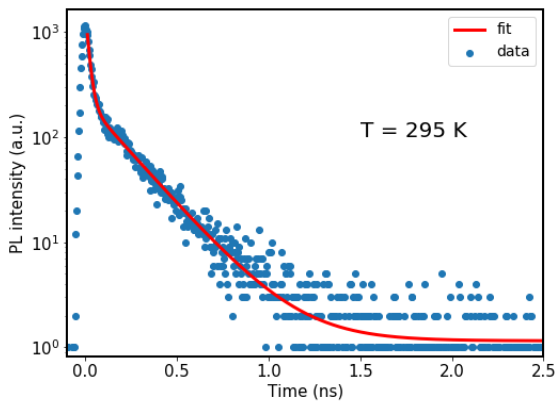
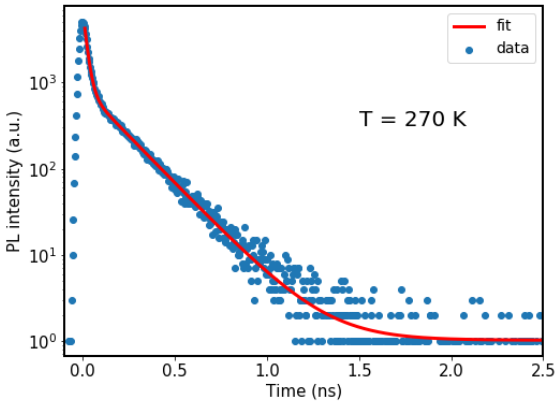
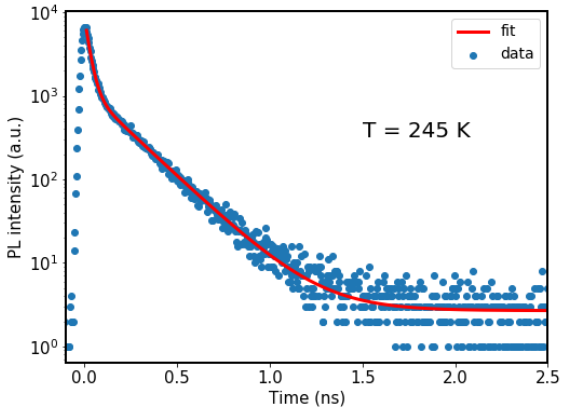
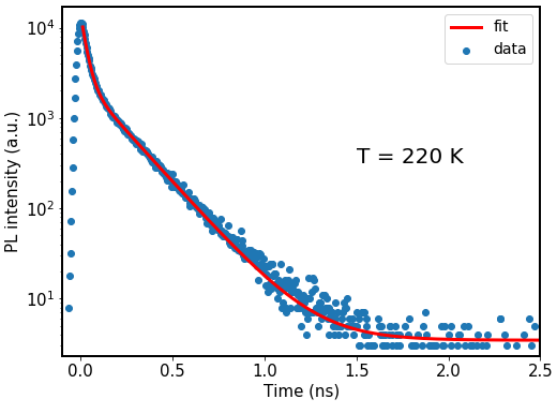


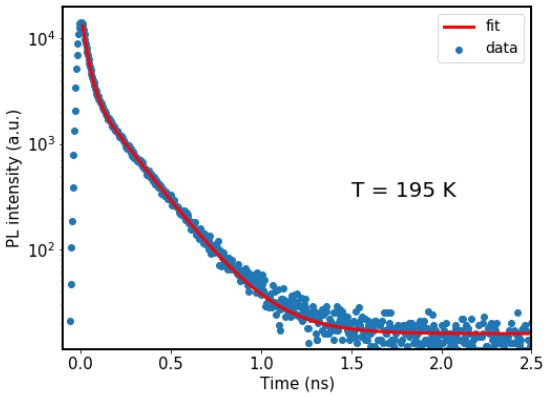
Figure S24. TIPL spectra of **4** at low temperature.

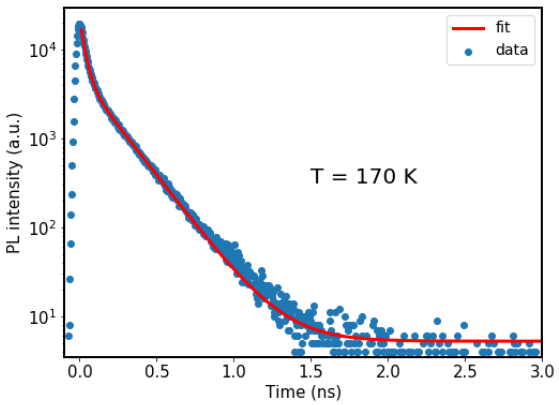

fit
data
T = 295 K
PL intensity (a.u.)
Time (ns)


fit
data
T = 270 K
PL intensity (a.u.)
Time (ns)


fit
data
T = 245 K
PL intensity (a.u.)
Time (ns)


fit
data
T = 220 K
PL intensity (a.u.)
Time (ns)


fit
data
T = 195 K
PL intensity (a.u.)
Time (ns)


fit
data
T = 170 K
PL intensity (a.u.)
Time (ns)

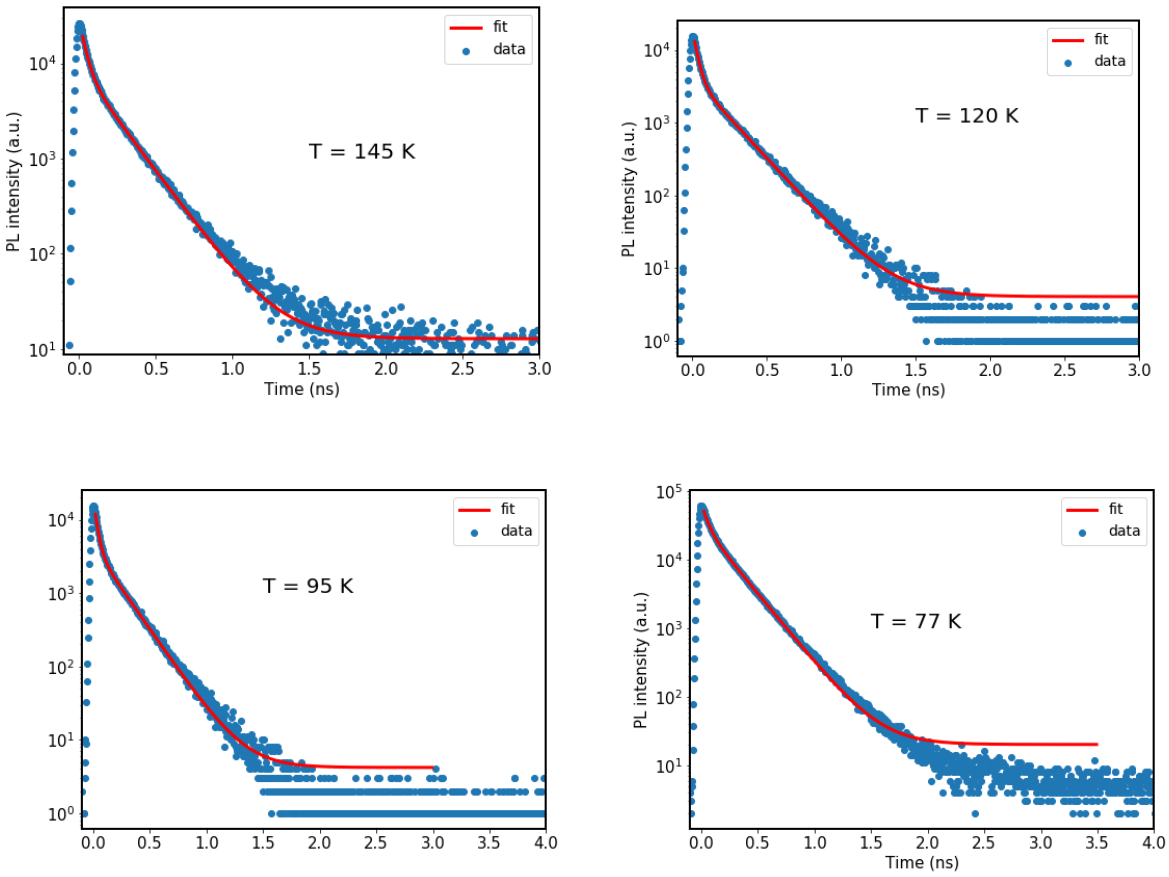


Figure S25. TRPL of **4** at low temperature.

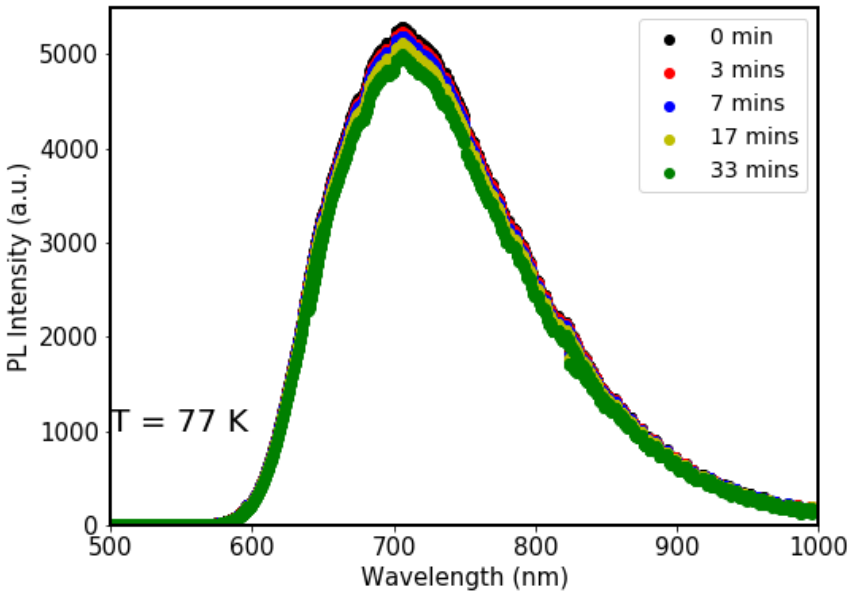


Figure S26. TIPL spectra of **8** at 77 K over time.

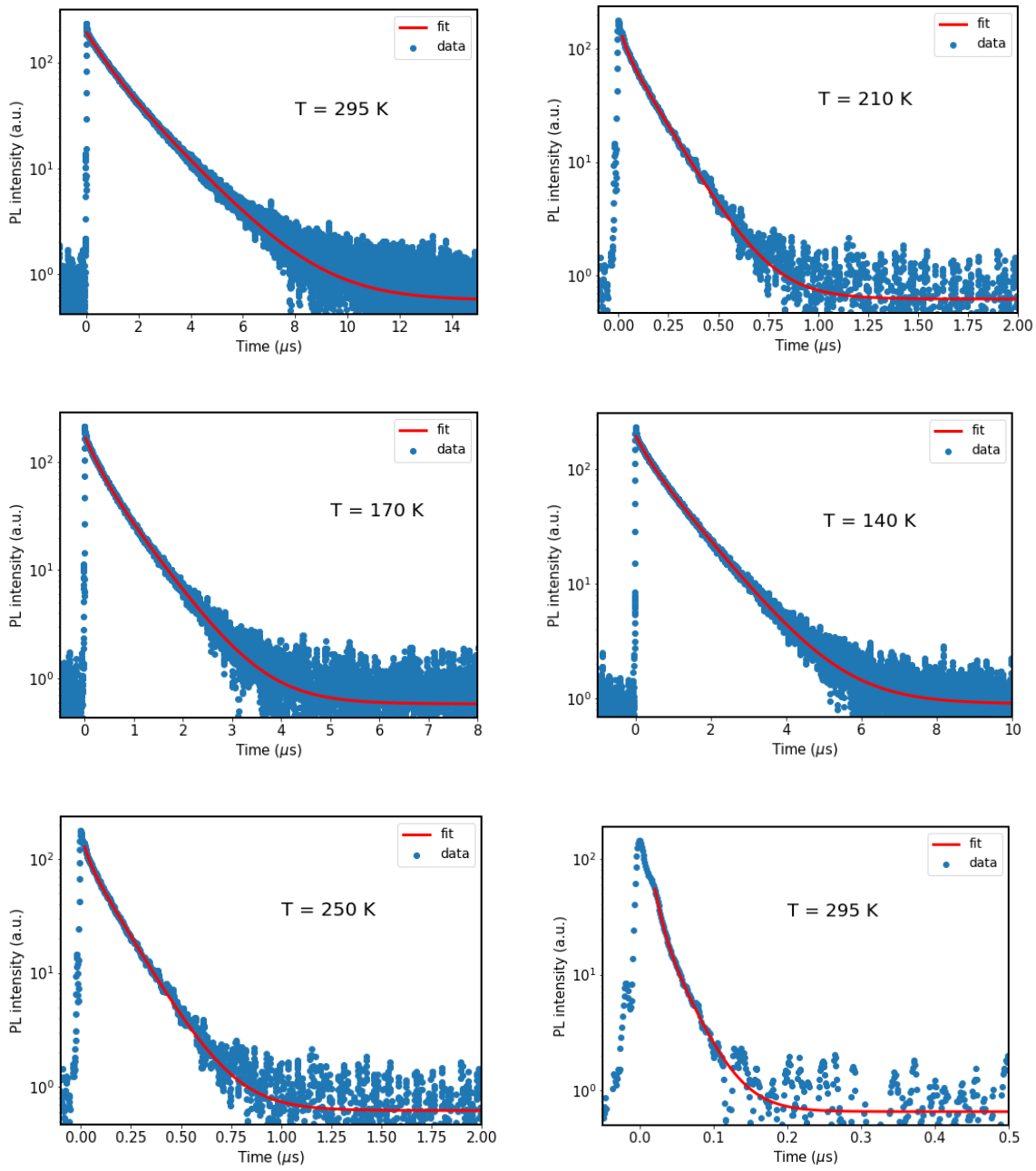


Figure S27. TRPL-μs of **8** at low temperature.

Computational Details

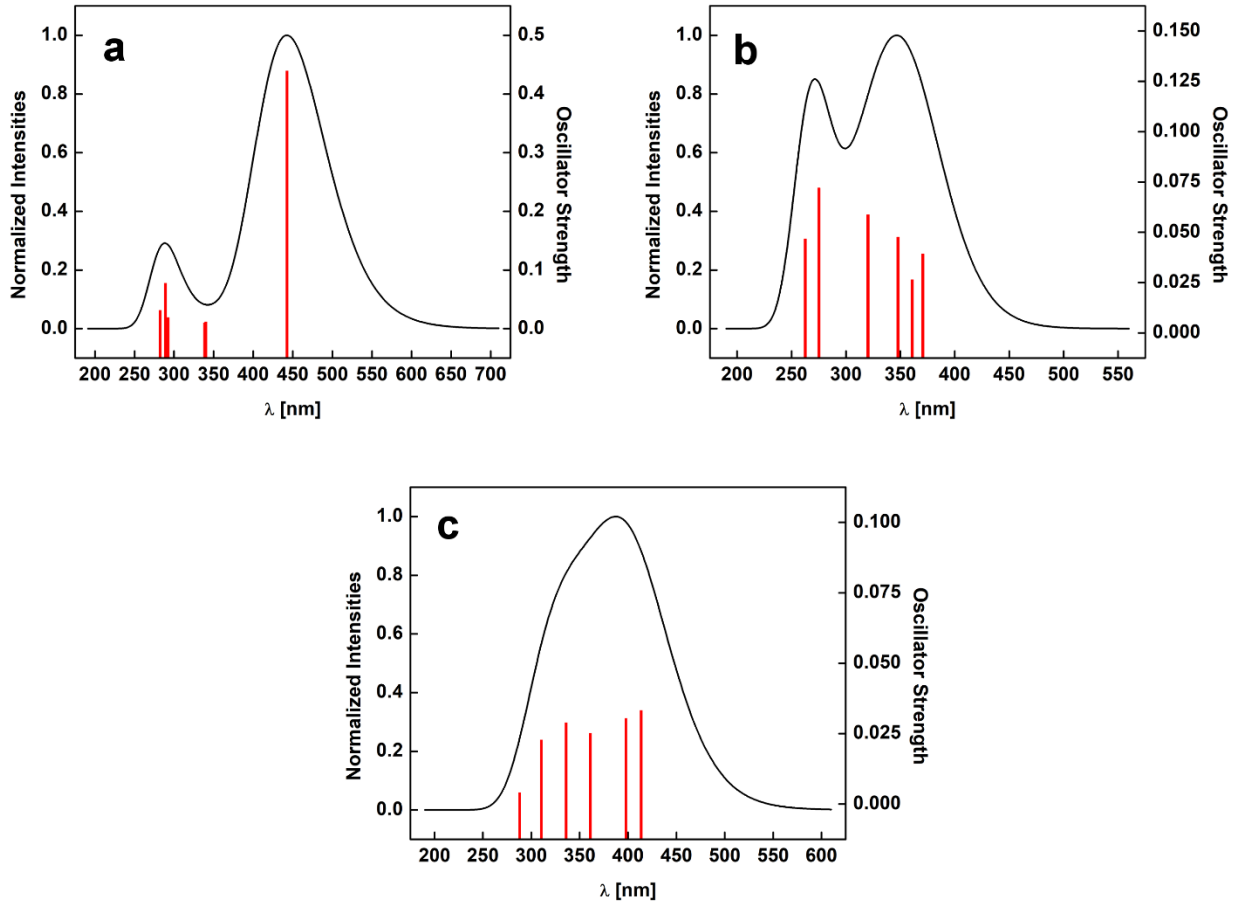


Figure S28. Calculated UV-vis spectra of **4** (a), **7** (b) and **8** (c) at the B3LYP/cc-pVTZ(-PP) level of theory including the six singlet excitation states with the highest oscillator strength (given as red bars).

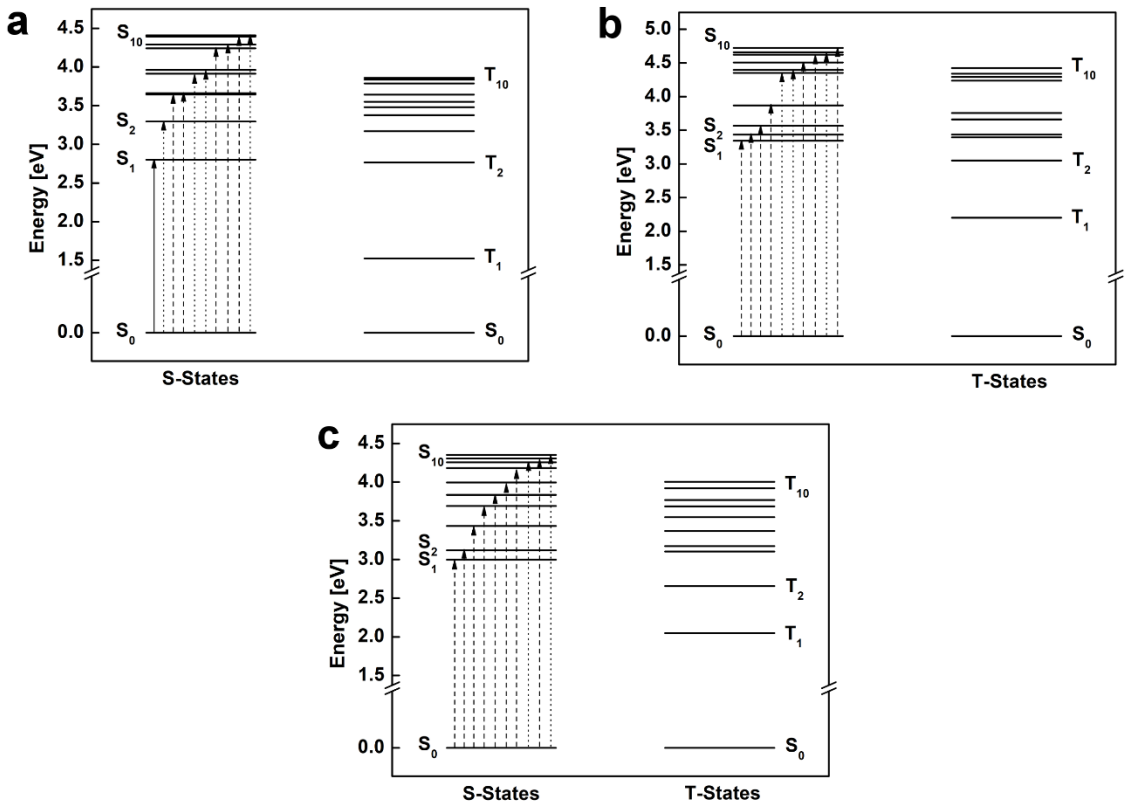


Figure S29. Calculated singlet and triplet states of **4** (a), **7** (b) and **8** (c) at the B3LYP/cc-pVTZ(-PP) level of theory. Oscillator strengths are indicated as follows: $f \geq 0.1$ (straight); $0.1 > f \geq 0.01$ (dashed); $0.01 > f \geq 0.001$ (dotted).

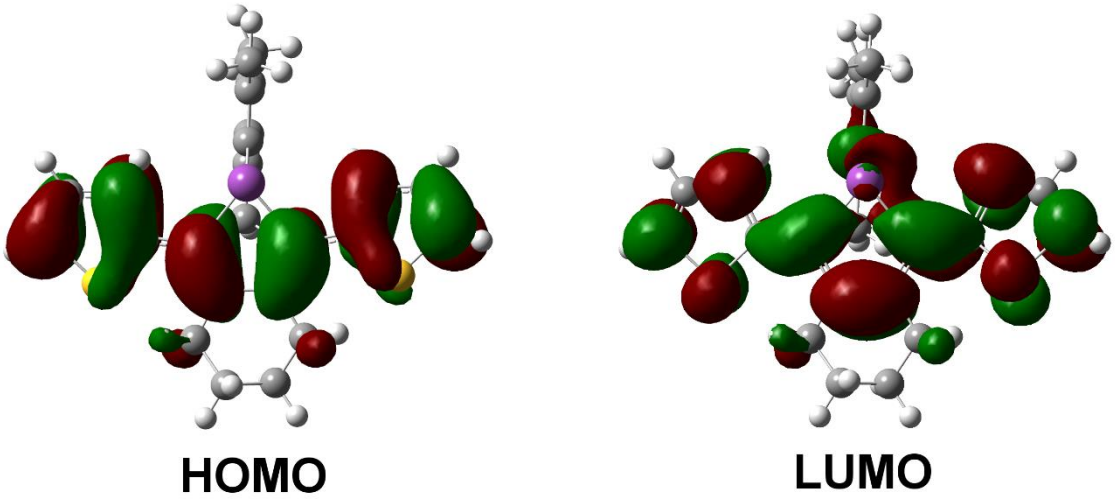


Figure S30. HOMO and LUMO of bismole **4**. MOs are calculated at the B3LYP/cc-pVTZ(-PP) level of theory and applying an *iso*-surface values of +0.02/–0.02 (red/green).

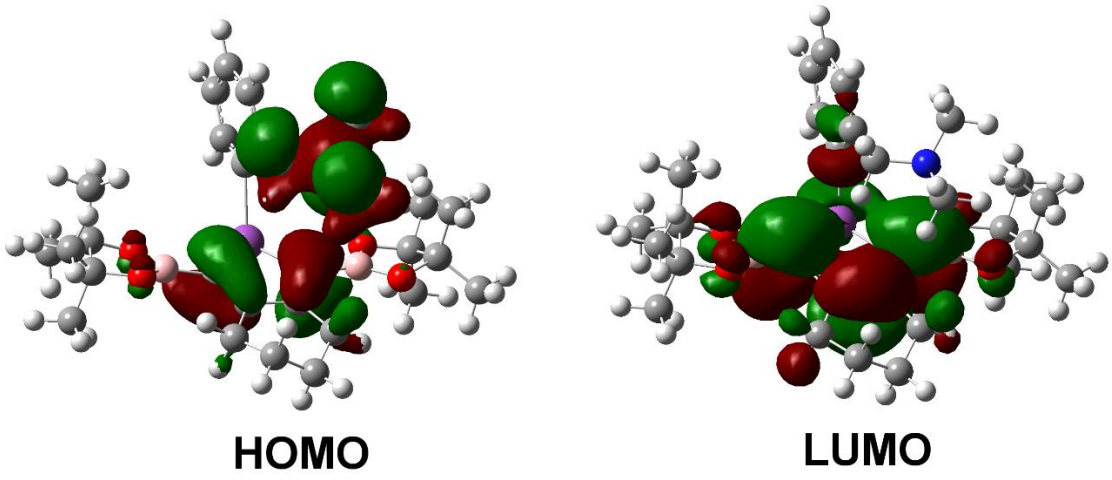


Figure S31. HOMO and LUMO of bismole **7**. MOs are calculated at the B3LYP/cc-pVTZ(-PP) level of theory and applying an *iso*-surface values of +0.02/–0.02 (red/green).

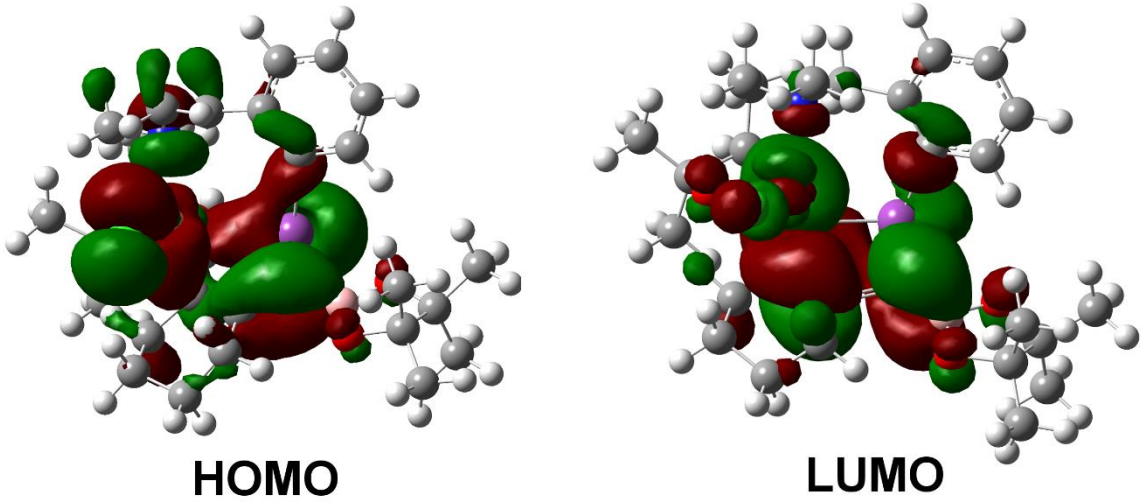


Figure S32. HOMO and LUMO of bismole **8**. MOs are calculated at the B3LYP/cc-pVTZ(-PP) level of theory and applying an *iso*-surface values of +0.02/–0.02 (red/green).

Table S6. TD-DFT calculated excited states of bismoles **4**, **7** and **8** at the B3LYP/cc-pVTZ(-PP) level of theory.

Excited States	**4** Energy [eV] and f	Excited States	**7** Energy [eV] and f	Excited States	**8** Energy [eV] and f
T_1	1.5246 0.0000	T_1	2.2000 0.0000	T_1	2.0489 0.0000
T_2	2.7663 0.0000	T_2	3.0511 0.0000	T_2	2.6573 0.0000
S_1	2.8012 0.4393	S_1	3.3452 0.0392	S_1	2.9981 0.0333
T_3	3.1691 0.0000	T_3	3.3947 0.0000	T_3	3.1023 0.0000
S_2	3.2943 0.0019	S_2	3.4362 0.0264	S_2	3.1174 0.0305
T_4	3.3781 0.0000	T_4	3.4369 0.0000	T_4	3.1736 0.0000
T_5	3.4801 0.0000	S_3	3.5651 0.0476	T_5	3.3706 0.0000
T_6	3.5492 0.0000	T_5	3.6611 0.0000	S_3	3.4351 0.0252
T_7	3.6433 0.0000	T_6	3.7580 0.0000	T_6	3.5474 0.0000
S_3	3.6460 0.0119	S_4	3.8706 0.0587	T_7	3.6865 0.0000
S_4	3.6615 0.0101	T_7	4.2355 0.0000	S_4	3.6913 0.0289
T_8	3.7862 0.0000	T_8	4.2929 0.0000	T_8	3.7696 0.0000
T_9	3.8358 0.0000	T_9	4.3411 0.0000	S_5	3.8369 0.0179
T_{10}	3.8587 0.0000	S_5	4.3529 0.0051	T_9	3.9205 0.0000
S_5	3.9124 0.0037	S_6	4.3971 0.0040	S_6	3.9946 0.0228
S_6	3.9633 0.0023	T_{10}	4.4212 0.0000	T_{10}	4.0033 0.0000
S_7	4.2412 0.0193	S_7	4.5071 0.0720	S_7	4.1824 0.0149
S_8	4.2895 0.0777	S_8	4.6230 0.0157	S_8	4.2564 0.0084
S_9	4.3926 0.0316	S_9	4.6586 0.0006	S_9	4.3062 0.0278
S_{10}	4.4084 0.0082	S_{10}	4.7220 0.0467	S_{10}	4.3526 0.0041

Table S7. TD-DFT calculated excited states of bismole **4** at B3LYP/TZ2P incl. SO coupling.

Ex. States	Energy [eV] and f	S-Weight	T-Weight	Ex. States	Energy [eV] and f	S-Weight	T-Weight
0	0.0000 0.5166E-08	99.9%	0.0%	21	3.6868 0.4419E-02	32.4%	67.3%
1	1.6326 0.1091E-04	0.0%	99.9%	22	3.7048 0.3672E-02	52.5%	46.8%
2	1.6327 0.6152E-06	0.0%	99.9%	23	3.7194 0.1995E-03	2.5%	97.2%
3	1.6328 0.3565E-05	0.0%	100.0%	24	3.7279 0.5974E-03	8.3%	91.5%
4	2.8128 0.4205	91.9%	7.9%	25	3.7609 0.5491E-02	38.8%	60.8%
5	2.8488 0.3188E-04	0.0%	99.8%	26	3.8003 0.4281E-04	0.3%	99.5%
6	2.8506 0.9059E-02	2.3%	97.6%	27	3.8019 0.5667E-04	0.4%	99.5%
7	2.8513 0.2026E-01	4.6%	95.2%	28	3.8062 0.1123E-02	7.6%	92.2%
8	3.1695 0.1183E-02	1.3%	98.6%	29	3.8607 0.9065E-05	0.0%	99.9%
9	3.1759 0.3486E-03	0.1%	99.7%	30	3.8608 0.6227E-05	0.0%	99.8%
10	3.1789 0.6604E-02	2.2%	97.6%	31	3.8626 0.1625E-03	1.5%	98.4%
11	3.2798 0.2036E-02	94.7%	5.1%	32	3.8813 0.6235E-04	0.4%	99.3%
12	3.3404 0.9803E-04	0.9%	98.9%	33	3.8815 0.9900E-04	0.6%	99.2%
13	3.3417 0.5878E-04	0.6%	99.1%	34	3.8825 0.3232E-03	2.4%	97.6%
14	3.3530 0.1343E-02	12.6%	87.1%	35	3.9045 0.4851E-02	99.2%	0.6%
15	3.4609 0.3008E-02	23.6%	76.3%	36	3.9485 0.2038E-02	99.4%	0.5%
16	3.5783 0.4283E-04	0.3%	99.4%	37	4.1586 0.5467E-01	98.1%	1.7%
17	3.5840 0.3110E-03	3.0%	96.6%	38	4.2917 0.3022E-01	97.8%	2.0%
18	3.6538 0.1295E-02	11.1%	88.7%	39	4.3902 0.1163E-01	99.8%	0.1%
19	3.6678 0.9970E-04	1.5%	98.3%	40	4.4059 0.1483E-01	99.7%	0.1%
20	3.6681 0.3343E-03	5.1%	94.7%				

Table S8. TD-DFT calculated excited states of bismole **7** at B3LYP/TZ2P incl. SO coupling.

Ex. States	Energy [eV] and f	S-Weight	T-Weight	Ex. States	Energy [eV] and f	S-Weight	T-Weight
0	0.0000 0.4233E-06	99.3%	0.5%	21	3.9526 0.2516E-02	8.7%	90.9%
1	2.3299 0.9397E-05	0.0%	99.9%	22	4.0161 0.3620E-01	61.7%	38.0%
2	2.3299 0.5576E-05	0.0%	99.99%	23	4.2590 0.2875E-03	0.9%	98.9%
3	2.3301 0.1869E-05	0.0%	99.9%	24	4.2623 0.4810E-03	1.6%	97.9%
4	2.9967 0.6880E-04	0.1%	99.7%	25	4.3089 0.3963E-03	4.6%	95.0%
5	2.9999 0.3804E-03	0.8%	99.1%	26	4.3166 0.2188E-03	0.5%	99.3%
6	3.0191 0.3884E-02	7.8%	92.0%	27	4.3315 0.1222E-03	0.6%	99.2%
7	3.2625 0.1506E-01	55.8%	44.0%	28	4.3326 0.3117E-03	1.5%	98.2%
8	3.3737 0.3184E-01	96.4%	3.4%	29	4.3642 0.1525E-02	12.7%	87.1%
9	3.4094 0.2110E-05	0.0%	99.8%	30	4.3754 0.8886E-04	0.3%	99.6%
10	3.4101 0.1080E-03	0.4%	99.5%	31	4.3782 0.2203E-03	2.8%	97.0%
11	3.4120 0.5461E-03	1.4%	98.4%	32	4.3878 0.5227E-02	84.5%	15.3%
12	3.5078 0.1040E-04	0.0%	99.9%	33	4.4112 0.2815E-02	94.4%	4.9%
13	3.5322 0.3513E-02	11.0%	88.8%	34	4.4643 0.1364E-02	3.7%	96.1%
14	3.5942 0.4319E-01	81.1%	18.8%	35	4.4949 0.1736E-02	8.1%	91.6%
15	3.6117 0.6350E-02	19.8%	79.5%	36	4.4960 0.4990E-03	1.0%	98.8%
16	3.7739 0.1964E-01	34.6%	65.1%	37	4.5935 0.6107E-01	92.0%	7.5%
17	3.8686 0.3411E-03	0.7%	98.9%	38	4.6712 0.1193E-01	96.6%	3.3%
18	3.8720 0.2267E-02	7.8%	92.0%	39	4.7043 0.7578E-02	93.7%	6.0%
19	3.9039 0.8275E-02	13.9%	85.9%	40	4.7627 0.4457E-01	96.2%	3.7%
20	3.9417 0.1330E-04	0.0%	99.8%				

Table S9. TD-DFT calculated excited states of bismole **8** at B3LYP/TZ2P incl. SO coupling.

Ex. States	Energy [eV] and f	S-Weight	T-Weight	Ex. States	Energy [eV] and f	S-Weight	T-Weight
0	0.0000 0.3564E-07	99.6%	0.2%	21	3.6179 0.9993E-03	3.7%	94.9%
1	2.1926 0.2671E-04	0.1%	99.7%	22	3.7008 0.2079E-01	70.1%	29.3%
2	2.1935 0.6131E-04	0.2%	99.6%	23	3.7992 0.5079E-02	27.3%	71.9%
3	2.1945 0.6607E-04	0.2%	99.6%	24	3.8102 0.1262E-02	6.6%	92.8%
4	2.6967 0.7481E-04	0.3%	99.4%	25	3.8191 0.2572E-02	9.6%	89.9%
5	2.6985 0.1239E-03	0.4%	99.3%	26	3.8563 0.7659E-03	3.4%	96.4%
6	2.7010 0.2979E-03	1.2%	98.7%	27	3.8711 0.1603E-03	0.6%	99.1%
7	2.9959 0.2718E-01	88.7%	11.1%	28	3.8749 0.1594E-02	7.5%	92.2%
8	3.0587 0.1831E-01	63.4%	36.0%	29	3.8905 0.7897E-02	41.8%	57.5%
9	3.1269 0.8926E-04	0.3%	99.5%	30	3.9694 0.5246E-02	22.6%	76.7%
10	3.1378 0.2926E-02	9.6%	90.2%	31	3.9760 0.6768E-03	3.0%	96.6%
11	3.1573 0.6942E-02	24.2%	75.2%	32	3.9846 0.3278E-02	15.4%	84.2%
12	3.2413 0.5327E-03	1.8%	98.0%	33	4.0065 0.8114E-02	36.8%	62.1%
13	3.2488 0.3067E-03	1.1%	98.9%	34	4.0974 0.6614E-02	29.5%	69.6%
14	3.2516 0.6052E-03	2.2%	97.7%	35	4.1247 0.6341E-03	2.9%	96.5%
15	3.3788 0.8398E-04	0.0%	99.0%	36	4.1442 0.5583E-02	23.1%	75.9%
16	3.3891 0.4056E-02	13.8%	84.9%	37	4.2498 0.1355E-01	89.3%	10.0%
17	3.3948 0.6982E-02	24.6%	74.7%	38	4.2765 0.5924E-02	97.7%	2.1%
18	3.4452 0.1739E-01	59.2%	38.3%	39	4.3129 0.2859E-01	98.4%	1.4%
19	3.5914 0.5150E-02	17.6%	81.9%	40	4.3565 0.4399E-02	97.1%	2.8%
20	3.6121 0.1521E-03	0.5%	98.7%				

Table S10. Calculated vertical, adiabatic and zero-point energies of **4**, **7** and **8**.

	4	**7**	**8**
S_0	–1979.1536 a.u.	–1752.3790 a.u.	–2410.0767 a.u.
ZPE(S_0)	0.4229 a.u.	0.689789 a.u.	0.6943 a.u.
T_1(UB3LYP)	–1979.1070 a.u.	–1752.3122 a.u.	–2410.0258 a.u.
ZPE(T_1/UB3LYP)	0.4201 a.u.	0.6877 a.u.	0.6923
E_{adia}	1.2681 eV	1.8199 eV	1.3856 eV
$E_{0\text{-}0}$	1.2164 eV	1.7628 eV	1.3310 eV

Table S11. Topological real space bonding indicators derived from the computed electron density of relevant bcps in bismoles **7** and **8**.

model	contact	d_1+d_2 [Å]	ρ(r) [eÅ^{-3}]	$\nabla^2\rho(r)$ [eÅ^{-5}]	d_1/d [%]	ε	G/ρ(r) [a.u.]	H/ρ(r) [a.u.]
8	Cu-Cl	2.214	0.54	5.8	45	0.04	1.04	–0.29
8	Cu-C(20)	2.436	0.59	5.6	42	1.11	0.96	–0.30
8	Cu-N	2.137	0.46	5.9	48	0.03	1.14	–0.24
8	C(2)-C(20)	1.407	2.06	–21.8	51	0.21	0.37	–1.11
8	C(1)-C(10)	1.354	2.31	–27.7	52	0.23	0.40	–1.24
7	C(2)-C(20)	1.355	2.30	–27.4	52	0.22	0.40	–1.23
7	C(1)-C(10)	1.354	2.31	–27.6	52	0.22	0.40	–1.24
8	Bi-C(20)	2.277	0.64	1.7	53	0.05	0.55	–0.37
8	Bi-C(10)	2.265	0.66	1.6	53	0.05	0.54	–0.38
8	Bi-C(31)	2.313	0.61	1.6	53	0.06	0.54	–0.36
7	Bi-C(20)	2.259	0.66	1.7	53	0.06	0.56	–0.38
7	Bi-C(10)	2.254	0.67	1.7	53	0.06	0.56	–0.38
7	Bi-C(31)	2.307	0.62	1.6	53	0.04	0.54	–0.36
8	C(20)-B(2)	1.547	1.31	–8.1	66	0.02	0.65	–1.08
8	C(10)-B(1)	1.539	1.32	–7.2	66	0.03	0.71	–1.09
7	C(20)-B(2)	1.537	1.32	–7.0	66	0.03	0.72	–1.09
7	C(10)-B(1)	1.537	1.33	–7.1	66	0.03	0.71	–1.09

For all bonds, $\rho(r)_{bcp}$ is the electron density at the bond critical point, $\nabla^2\rho(r)_{bcp}$ is the corresponding Laplacian, ε is the bond ellipticity, $G/\rho(r)_{bcp}$ and $H/\rho(r)_{bcp}$ are the kinetic and total energy density over $\rho(r)_{bcp}$ ratios.

Table S12. ELI-D basin properties of bismole **7** and **8**.

model	basin	N_{ELI} [e]	V_{ELI} [Å^3]	γ_{ELI}	Δ_{ELI} [Å]	model	basin	N_{ELI} [e]	V_{ELI} [Å^3]	γ_{ELI}	Δ_{ELI} [Å]
7	C(2)-C(20)	3.10	10.31	1.77	0.05	**8**	C(2)-C(20)	2.66	5.26	1.79	0.15
7	C(1)-C(10)	3.11	9.99	1.77	0.12	**8**	C(1)-C(10)	3.14	11.08	1.77	0.14
7	Bi-C(20)	1.86	6.24	1.65	0.16	**8**	Bi-C(20)	2.41	7.48	1.63	0.17
7	Bi-C(10)	1.86	6.41	1.65	0.16	**8**	Bi-C(10)	1.83	6.08	1.64	0.09
7	Bi-C(31)	2.01	8.92	2.08	0.16	**8**	Bi-C(31)	1.99	7.80	1.76	0.15
7	C(20)-B(2)	2.46	8.97	1.74	0.06	**8**	C(20)-B(2)	2.46	8.05	2.07	0.05
7	C(10)-B(1)	2.44	8.36	2.09	0.05	**8**	C(10)-B(1)	2.46	8.87	2.08	0.04
7	Bi(LP)	2.63	24.84	1.58	-	**8**	Bi(LP)	2.67	25.21	1.52	-
						8	Cu-N	2.15	4.66	1.87	0.08

Table S13. AIM atomic charges and Wiberg Bond-Indices derived from NBO analysis of **7** and **8**.

Atom	model	Q [e]	model	Q [e]	Contact	model	WBI	model	WBI
C(20)	**7**	–0.99	**8**	–1.07	C(2)-C(20)	**7**	1.75	**8**	1.51
C(2)	**7**	–0.04	**8**	–0.08	C(1)-C(10)	**7**	1.76	**8**	1.76
C(1)	**7**	–0.04	**8**	–0.03	Bi-C(20)	**7**	0.81	**8**	0.76
C(10)	**7**	–0.99	**8**	–1.07	Bi-C(10)	**7**	0.81	**8**	0.78
Bi	**7**	1.00	**8**	0.99	Bi-C(31)	**7**	0.79	**8**	0.82
N	**7**	–0.92	**8**	–0.91	C(20)-B(2)	**7**	0.98	**8**	0.94
Cu			**8**	0.66	C(10)-B(1)	**7**	0.97	**8**	0.97
Cl			**8**	–0.68	Cu-Cl			**8**	0.57
					Cu-C(20)			**8**	0.26
					Cu-C(2)			**8**	0.25
					Cu-N			**8**	0.15

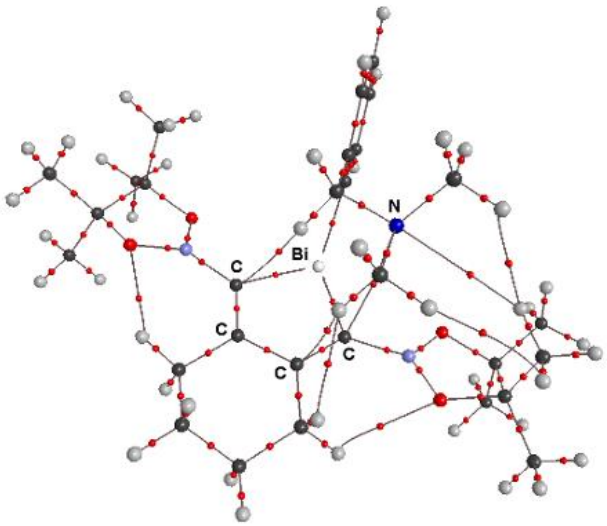


Figure S33. AIM bond paths motifs of bismole **7**.

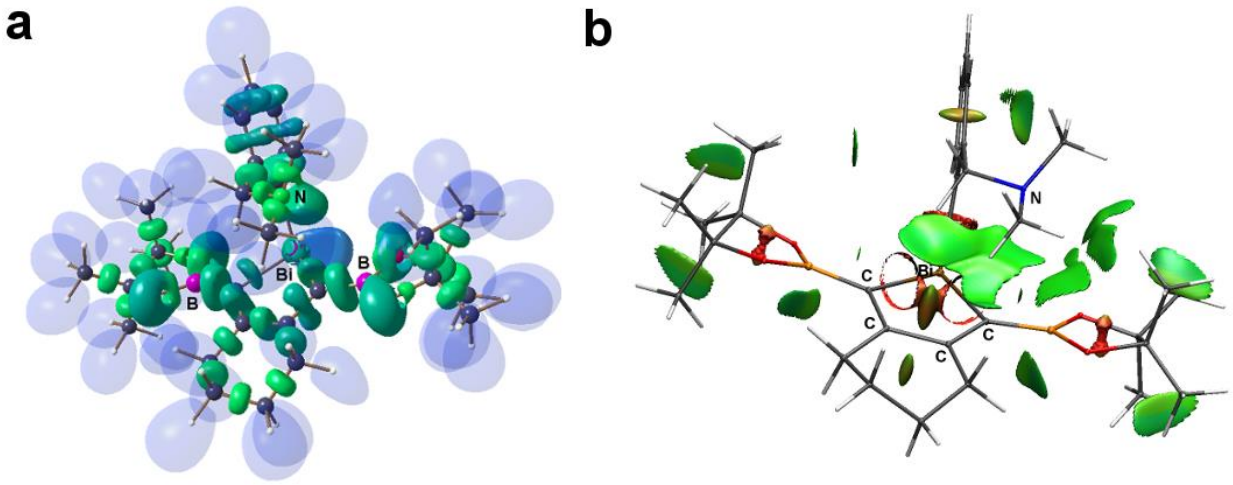


Figure S34. a) *Iso*-surface representation of the localization domains of the ELI-D (Y = 1.4) of **7**. The basins are color coded from green (small) to blue (large); b) NCI *iso*-surfaces (s(**r**) = 0.5; attractive/repulsive non-covalent bonding aspects given in blue/red).

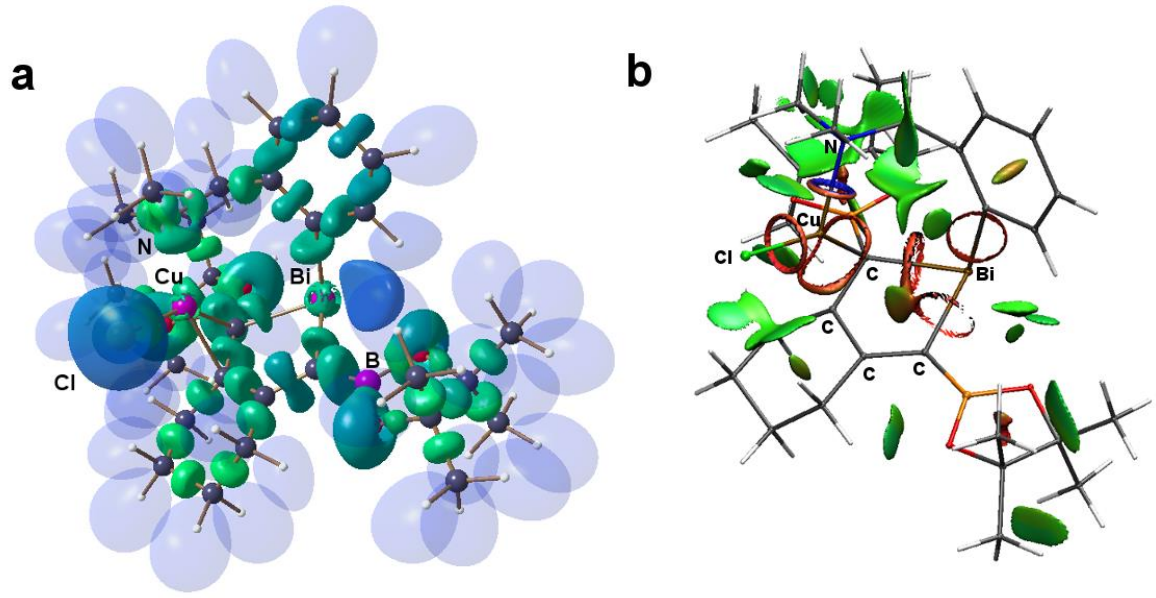


Figure S35. a) *Iso*-surface representation of the localization domains of the ELI-D (Y = 1.4) of **8**. The basins are color coded from green (small) to blue (large); b) NCI *iso*-surfaces (s(**r**) = 0.5; attractive/repulsive non-covalent bonding aspects given in blue/red.